Quantitative Proteomics and Phosphoproteomics Supports a Role for Mut9-Like Kinases in Multiple Metabolic and Signaling Pathways in *Arabidopsis*

Margaret E. Wilson[1], Shin-Cheng Tzeng[1], Megan M. Augustin[1], Matthew Meyer[1], Xiaoyue Jiang[2], Jae H. Choi[3], John C. Rogers[2], Bradley S. Evans[1], Toni M. Kutchan[1], Dmitri A. Nusinow[1*]

[1]Donald Danforth Plant Science Center, St. Louis, MO, 63132, USA

[2]Thermo-Fisher Scientific, San Jose, CA, 95134, USA

[3]Thermo-Fisher Scientific, Rockford, IL, 61101 USA

***To whom correspondence should be addressed** dnusinow@danforthcenter.org

Running Title: Quantitative Proteomic Analysis of MLK Family Kinases

Summary/Abstract

Protein phosphorylation is one of the most prevalent post-translational modifications found in eukaryotic systems and serves as a key molecular mechanism by which protein function is regulated in response to environmental stimuli. The Mut9-Like Kinases (MLKs) are a plant-specific family of Ser/Thr kinases that have been linked to light, circadian, and abiotic stress signaling. Here we use quantitative phosphoproteomics in conjunction with global proteomic analysis to explore the role of the MLKs in daily protein dynamics. In the absence of MLK family kinases, proteins involved in light, circadian, and hormone signaling as well as several chromatin modifying enzymes were found to have altered phosphorylation profiles. Additionally, *mlk* mutant seedlings were found to have elevated glucosinolate accumulation and increased sensitivity to DNA damage. Our analysis in combination with previously reported data supports the involvement of MLKs in a diverse set of stress responses and developmental processes, suggesting that the MLKs may serve as key regulators linking environmental inputs to developmental outputs.

Introduction

Protein phosphorylation is one of the most prevalent and well-studied post-translational modifications occurring in eukaryotic cells. This dynamic modification is key in regulating protein function and turnover, making it an integral part of complex signaling networks and regulatory processes. Rapid and reversible post-translational regulation is advantageous to plants, as they are often required to quickly adapt to changing environments. Moreover, protein phosphorylation is at the core of various biological processes including stress response, light signaling, circadian regulation, and hormone perception and transduction. In Arabidopsis, nearly 4% of protein encoding genes are kinases (Wang et al., 2014), which is a testament to the importance of phosphorylation-based protein regulation. Despite the upswing of large-scale phosphoproteomic studies in plant species (Silva-Sanchez et al., 2015), a recent study suggests that the identification

of Arabidopsis phosphoproteins and phosphosites is far from comprehensive (Vlastaridis et al., 2017).

Recently, a four-member family of Ser/Thr protein kinases known as the MUT9-like kinase/Photoregulatory Protein Kinases/Arabidopsis EL1-like (MLK/PPK/AEL) kinases, herein referred to as the MLKs, has been shown to be involved in the phosphoregulation of several key signaling proteins (Ni et al., 2017; Liu et al., 2017; Su et al., 2017; Chen et al., 2018). The MLKs are a plant and green algae-specific family of kinases related to casein kinase I (CKI). The MLKs show significant divergence from CKI, as similarities are restricted to their catalytic domains (Casas-Mollano et al., 2008). MLK family kinases are capable of phosphorylating histones H3 and H2A in *Arabidopsis* as well as the green algae *Chlamydomonas*. The *Chlamydomonas* MLK orthologue, MUT9, is also required for transgene silencing and response to DNA damaging agents (Casas-Mollano et al., 2008; Jeong Br et al., 2002). In addition to phosphorylating histones, MLK family kinases phosphorylate proteins involved in multiple signaling pathways. Early studies of a rice MLK orthologue, EARLY FLOWERING1 (EL1), have linked this kinase family to hormone signaling and the regulation of flowering time (Dai and Xue, 2010), a role which is at least in part conserved in *Arabidopsis* (Zheng et al., 2017; Chen et al., 2018; Huang et al., 2016). MLKs also interact with core components of the morning (Zheng et al., 2017; Su et al., 2017) and evening (Huang et al., 2016) loops of the *Arabidopsis* circadian clock. The association of the MLKs with the evening complex components, EARLY FLOWERING 3 AND 4 (ELF3 and ELF4) is dependent on the presence of the red light receptor phytochrome B (Huang et al., 2016). Additionally, the MLKs are capable of phosphorylating the blue light receptor CRYPTOCHROME2 and the red light-regulated transcription factor PHYTOCHROME INTERACTING FACTOR 3 (Ni et al., 2017; Liu et al., 2017). Taken together, these studies suggest that the MLKs provide a link between light and circadian signaling, which in turn regulates subsequent growth and development.

74 In this study, we used quantitative phosphoproteomic techniques to expand our understanding of
75 the various signaling pathways and cellular protein networks the MLK family of kinases
76 participate in. We combined isobaric labeling with high pH reversed-phase prefractionation and
77 TiO_2 based phosphopeptide enrichment to achieve an in-depth phosphoproteomic analysis of
78 wild-type and *mlk* mutant seedlings at two different time points, one at the end of the day (ZT12)
79 and the other several hours into the night (ZT14). Over 20,000 phosphosites mapping to nearly
80 5,000 protein groups were identified. In the MLK mutant backgrounds, enzymes involved in
81 glucosinolate metabolism were altered in abundance and proteins involved in a diverse set of
82 biological processes including RNA processing, chromatin organization, and stress responses
83 were differentially phosphorylated. The confluence of stress and chromatin factors suggested that
84 MLKs may also be involved in regulating DNA-damage responses in *A. thaliana*. This hypothesis
85 was addressed by assessing the sensitivity of *mlk* mutants to DNA-damaging agents.

86 **Experimental Procedures**

87 **Plant Material**

88 The *mlk1* (SALK_002211; AT5G18190), *mlk2* (SALK_064333; AT3G03940), and *mlk3*
89 (SALK_017102; AT2G25760) mutant lines were obtained from the ABRC (Ohio State University).
90 The *mlk4* (GABI_756G08; AT3G13670) mutant line was obtained from the Nottingham
91 Arabidopsis Stock Centre. All are in the Colombia (Col-*0*) background and were isolated as
92 previously described (Huang et al., 2016).

93 **Tissue Collection for Mass Spectrometry**

94 Arabidopsis wild type (Col-*0*) and mutant seedlings were grown on sterilized qualitative filter paper
95 (Whatman) overlaid on ½ x MS (Murashige and Skoog) plates containing 1% sucrose and 0.8%
96 agar at 22˚C. Seedlings were entrained under 12 h white light (100-110 μmol/m^2/s)/12 h dark

97 cycle. Tissue was collected on the 10th day of growth immediately prior to lights off [Zeitgeber 12,
98 (ZT12)] and after 2h of dark (ZT14).

99 **Protein Isolation and Digestion**

100 The seedlings were transferred into a liquid N_2 chilled 35ml ball mill and disrupted in a reciprocal
101 mixer mill [30 hz, 45 seconds, repeated 3 times (Retsch USA)] under liquid nitrogen. Ground
102 tissue was gently resuspended in 1 mL (approximately 1 packed tissue volume) of SII buffer (100
103 mM sodium phosphate, pH 8.0, 150 mM NaCl, 5 mM EDTA, 5 mM EGTA, 0.1% Triton X-100, 1
104 mM PMSF, 1x protease inhibitor cocktail [Roche], 1x Phosphatase Inhibitors II & III [Sigma], and
105 50 μM Mg-132 [Peptides International]) and sonicated twice at 40% power, 1 second on/off cycles
106 for 20 s total on ice (Fisher Scientific model FB505, with microtip probe). Extracts were clarified
107 by centrifugation twice at 4˚C for 10 min at ≥20,000xg. Protein concentrations were determined
108 by BCA protein assay (Thermo-Fisher Scientific, Rockford, IL). Protein samples were reduced
109 with 10 mM TCEP and alkylated with 25 mM iodoacetamide prior to trypsin digestion in 1/40
110 enzyme/protein ratio at 37°C overnight.

111 **Phosphopeptide Enrichment**

112 Phosphopeptide enrichment was performed using the High-Select™ TiO_2 Phosphopeptide
113 Enrichment kit (Thermo Scientific PN32993) following vendor's protocol. Briefly, dried peptides
114 were reconstituted in 150 μL of binding/equilibration buffer provided and applied to the TiO_2 spin
115 that was previously equilibrated with binding buffer/equilibration. After reapplying sample once,
116 the tip was sequentially washed twice with 20 μL of binding buffer and wash buffer, and once with
117 20 μL of LC-MS grade water. Bound peptides were eluted by two applications of 50 μL of elution
118 buffer (also provided). Eluates containing the enriched phosphopeptides were dried down and
119 subsequently resuspended with 50 μl 0.1% formic acid for peptide concentration measurement
120 using the Pierce Quantitative Colorimetric Assay kit (Thermo Scientific PN23275).

121 **Tandem Mass Tag (TMT) Labeling**

122 100 µg of each digested sample was added to 100 µL of 100 mM HEPES pH 8.5 buffer. A
123 reference pooled sample composed of equal amounts of material from all samples was also
124 generated to link TMT experiments. Isobaric labeling of the samples was performed using 10-plex
125 tandem mass tag (TMT) reagents (Thermo Fisher Scientific, Rockford, IL). All individual and
126 pooled samples were labeled according to the TMT 10-plex reagent kit instructions. Briefly, TMT
127 regents were brought to room temperature and dissolved in anhydrous acetonitrile. Peptides
128 were labeled by the addition of each label to its respective digested sample. Labeling reactions
129 were incubated for 1 h at room temperature. Reactions were terminated with the addition of
130 hydroxylamine.

131 **High pH Reverse Phase Fractionation**

132 High pH reverse phase fractionation was performed using the Pierce High pH Reversed-Phase
133 Peptide Fractionation Kit (Thermo Scientific PN84868) according to manufacturer's instructions.
134 Briefly, peptide samples were dissolved in 300 µL of 0.1% TFA solution in LC-MS grade water.
135 and subsequently loaded onto reversed-phase fractionation spin columns also equilibrated with
136 0.1% TFA. Samples were then washed with 300 µL of 5% ACN/ 0.1% TEA to remove unreacted
137 TMT reagent. Peptides were eluted into 8 peptide fractions with an ACN step gradient (i.e. 10%,
138 12.5%, 15%, 17.5%, 20%, 22.5%, 25%, and 50%). Samples were acidified and dried down prior
139 to LC-MS.

140 **LC-MS/MS Analysis**

141 Two microliters (one microgram) of sample was injected onto a 0.075 x 500 mm EASY-Spray
142 Pepmap C18 column equipped with a 0.100 x 5 mm EASY-Spray Pepmap C18 trap column
143 (Thermo-Fisher Scientific, San Jose, CA) attached to an EASY-nLC 1000 (Thermo-Fisher
144 Scientific, San Jose, CA). The peptides were separated using water (A) and acetonitrile (B)

145 containing 0.1% formic acid as solvents at a flow rate of 300 nL per minute with a three-hour
146 gradient. Data were acquired in positive ion data dependent mode on an Orbitrap Fusion Lumos
147 mass spectrometer (Thermo-Fisher Scientific, San Jose, CA) with a resolution of 120,000 (at *m*/*z*
148 200) and a scan range from *m*/*z* 380-1500. Precursor isolation was performed using the
149 quadrupole prior to either CID activation in the ion trap and detection in the Orbitrap at a resolution
150 of 30,000 or HCD activation with detection in the Orbitrap at a resolution of 60,000.

151 **Data Analysis**

152 All MS/MS data were analyzed using Proteome Discoverer 2.1 (Thermo-Fisher Scientific, San
153 Jose, CA). The search algorithm used in the study was Byonic v2.11 as part of the Proteome
154 Discoverer software platform. Precursor ion mass tolerance was set to 10 ppm, fragment ion
155 tolerance was 20 ppm; up to 2 missed cleavages were allowed. Carbamidomethylation (+57.021
156 Da) on cysteine and TMT tag (+229.163 Da) on peptide N-termini as well as lysine residues were
157 set as static modifications. Dynamic modifications included acetylation (+42.011 Da) on protein
158 N-termini, oxidation (+15.995 Da) on methionine and phosphorylation (+79.966 Da) on serine,
159 threonine, and tyrosine. Data were searched against TAIR10 database (20101214, 35,386
160 entries) with FDR set to 1%.

161 For quantitation, reporter ion intensity integration tolerance was set to 20 ppm. Reporter ion
162 abundances were corrected for isotopic impurities based on manufacturer's specifications. For
163 each peptide, a minimal average reporter S/N threshold of 2 and a co-isolation threshold of 100%
164 are required. The S/N values for all peptides were summed within each TMT channel, and each
165 channel was scaled according to the reference channel. Both unique and razor peptides were
166 used for quantification.

167 Peptides of altered abundance were identified from the Byonic output list generated from HCD
168 MS2 analysis using Microsoft Excel. Abundance ratios for mutant/wild type pairwise comparisons

169 were calculated from the average peptide abundance of mutant and wild-type biological
170 replicates. Only peptides identified in at least 2 biological replicates were considered for further
171 analysis. Statistical significance was determined by Student's *t*-test (*P*-value ≤ 0.05).

172 **Bioinformatic Analysis**

173 The Motif-X algorithm (Chou and Schwartz, 2011) was used to extract significantly enriched
174 phosphorylation motifs from *mlk1/2/3* and *mlk1/3/4* phosphopeptide data sets. Only
175 phosphopeptides with high confidence phosphorylation sites were used in analysis. The peptides
176 were aligned and extended to a width of 15 amino acids using the online utility
177 PEPTIDEXTENDER ver.0.2.2 alpha (schwartzlab.uconn.edu/pepextend/). The aligned peptides
178 were used to extract motifs. The probability threshold was set to p-value ≤ 10^{-5}; the occurrence
179 threshold was set to 10. The default IPI Arabidopsis Proteome data set was used as the
180 background data set.

181 Enrichment analysis of Gene ontology (GO) categories was performed with g:Profiler (Reimand
182 et al., 2016). AGI accession numbers for Arabidopsis were uploaded to the g:Profiler webserver
183 (http://biit.cs.ut.ee/gprofiler/) and GO enrichment was determine using default settings
184 (significance level 0.05). Enriched terms were summarized and redundancy removed using the
185 online tool REVIGO (Supek et al., 2011). Semantic similarity threshold (dispensability) was set to
186 0.5 (default) for all global proteome analysis and cellular component category of the
187 phosphoproteome analysis. Dispensability was increased to 0.7 for all other analysis.

188 **Glucosinolate Extraction and Analysis by HPLC and LC-MS/MS**

189 Arabidopsis seeds (Col-0*, mlk 1/2/3,* and *mlk 1/3/4*) were sown on ½ x MS (Murashige and Skoog)
190 plates containing 1% sucrose and 0.8% agar and grown under 12 h white light (100-110
191 μmol/m^2/s)/12 h dark cycle at 22˚C for 10 days prior to harvest at ZT12. Glucosinolates were
192 extracted from approximately 350 mg of whole seedlings and desulfonated (in quadruplicate) as

193 previously described (Crocoll *et al.* 2016) using sinigrin as an internal standard. Desulfo-GLS
194 extracts were analyzed by HPLC (Waters) equipped with a photodiode array detector and
195 separated using a Gemini C-18 column (150 X 2.00 mm, 5 µm; Phenomenex) with a flow rate of
196 0.5 mL per minute and the following solvents and binary gradient: solvent A-water and solvent B-
197 acetonitrile; where solvent B was held at 1.5% for 1 min, then 1-6 min 1.5-5% B, 6-8 min 5-7% B,
198 8-18 min 7-21% B, 18-23 min 21-29% B, 23-30 min 29-43% B, 30-33 min 43-100% B, 33-37 100%
199 B, 37-38 min 100-1.5% B, and held at 1.5% B for an additional 7 minutes. GLS peaks were
200 identified using previously published UV spectra in addition to reported relative retention times
201 and quantitated using peak areas of desulfo-GLS and internal standard along with published
202 response factors (Brown *et al.* 2003, Grosser and Dam 2017). GLS identities were confirmed by
203 LC-MS/MS (SCIEX 6500 QTRAP, Framingham, MA) using enhanced product ion (EPI; ion trap
204 MS/MS) scans to verify the presence of previously published fragment ions (Crocoll et al. 2016)
205 from each glucosinolate ion. Mass spectrometric data were collected in positive ion mode using
206 the same gradient/solvents/column as for HPLC-UV analysis with the following source conditions:
207 curtain gas, 20; ion-spray voltage, 5500 V; temperature, 500° C; gas 1, 40; gas 2, 45; declustering
208 potential, 80 V; entrance potential, 10 V; collision energy 20 eV.

209 **MMS Treatment**

210 Arabidopsis wild type (Col-*0*) and mutant seed was surface-sterilized and sown on ½ x MS
211 (Murashige and Skoog) plates containing 1% sucrose and 0.8% agar with or without methyl
212 methanesulfonate (MMS, Sigma). After stratification for 2 days at 4°C, seedlings were grown
213 under 12 h white light (100-110 µmol/m^2/s)/12 h dark cycle at 22˚C. For growth sensitivity assays,
214 seedlings were germinated on control media and after 5 days of growth were transferred to MMS
215 treatment media. Fresh weight was measured after 15 days of growth in the presence of MMS.
216 For post-germination developmental assessment, seed was germinated on ½ x MS plates

217 containing 1% sucrose, 0.8% agar, and 150 ppm MMS. Seedlings were imaged and scored for
218 arrest at 12 days after germination.

219 **UV-C Tolerance Assay**

220 Whole-plant sensitivity to UV-C (254 nm) was evaluated as described in Castells et al. (2010) with
221 the following modifications. 8-day old seedlings were irradiated with 2000 or 4000 J m^{-2} of UV-C
222 twice during a 48 hr time period using a Stratalinker® UV Crosslinker 1800. Following each
223 treatment, plants were returned to growth conditions of 12 h white light (100-110 μmol/m^2/s)/12 h
224 dark cycle at 22˚C. After 5 days of recovery, phenotypes were measured and seedlings were
225 imaged.

226

227 **Results**

228 **Proteomic Analysis Reveals Changes in Stress Response Pathways in *mlk* Mutant**
229 **Seedlings**

230 Tandem mass tag (TMT) labeling combined with high pH reversed-phase fractionation and
231 tandem mass spectrometry was used to quantify the regulatory effects of the MLKs on proteome
232 dynamics (**Fig. 1**). Wild-type and *mlk* mutant *Arabidopsis* seedlings were entrained under 12 h
233 light and 12 h dark conditions. We compared *mlk1/2/3* and *mlk1/3/4* mutant seedlings, as we were
234 unable to isolate viable *mlk1/2/3/4* mutant seed (Huang et al., 2016; Liu et al., 2017). This mutant
235 combination will allow us to assess potential redundancy within the MLK family and facilitate the
236 identification of *mlk2* or *mlk4* specific changes. As the MLKs have been previously associated
237 with light-signaling pathways, we collected tissue either immediately prior to lights off [Zeitgeber
238 12, (ZT12)] or after 2h of dark (ZT14). We identified nearly 50,000 peptides combined, mapping
239 to over 7,500 protein groups at both ZT12 and ZT14. Pairwise comparisons between *mlk* mutants
240 and WT were performed to identify peptides showing altered abundance in the MLK mutant
241 backgrounds at both the ZT12 and ZT14 time-points (**Supplemental Dataset S1**). Peptides were

242 classified as altered in abundance if both the $\log_2$ FC was at least ±1 (2 fold-change) and the p-
243 value < 0.05. Only 13 unique proteins met our altered abundance criteria in the *mlk1/2/3* mutant
244 when compared to wild type at both ZT12 and ZT14 (**Fig. 2 and Supplemental Table S1**). In the
245 *mlk1/3/4* mutant background, more than 225 peptides mapping to over 110 unique proteins were
246 found to meet our altered abundance threshold at ZT12 and ZT14 when compared to wild type
247 (**Fig. 2 and Supplemental Table S1**). These results suggest that the *mlk1/3/4* mutant
248 combination has a greater impact on the global proteome than the *mlk1/2/3* mutant combination
249 at the light-to-dark transition.

250 **Quantitative Phosphoproteomic Comparisons of *mlk* Mutants**

251 The MLKs have been shown to physically interact with and phosphorylate important regulatory
252 proteins (Liu et al., 2017; Chen et al., 2018; Dai and Xue, 2010; Ni et al., 2017). Thus, to gain
253 insight into the role of the MLKs in global phosphorylation, we characterized the
254 phosphoproteome of wild type, *mlk1/2/3,* and *mlk1/3/4* mutant seedlings in the light (ZT12) and
255 after transition to dark (ZT14). We applied a TiO_2 based phosphopeptide enrichment technique to
256 the TMT-10plex labeled samples described above to achieve an in-depth phosphoproteomic
257 analysis using the Thermo Scientific Orbitrap Fusion Lumos Tribrid mass spectrometer **(Fig. 1)**.
258 Byonic software, run as a node within the Proteome Discover V2.1 platform was used to identify
259 and derive relative quantitation for phosphoproteins. Using this strategy, a combined total of
260 23,386 phosphosites on 15,222 unique peptides mapping to 4,854 protein groups were identified
261 at ZT12. Slightly fewer were identified at ZT14, with 19,947 phosphosites on 12,818 unique
262 peptides mapping to 4,467 protein groups being identified. At ZT12, over 80% of the identified
263 phosphosites were serine residues, approximately 15% were threonine, and less than 2% were
264 tyrosine (**Fig. 3A**), which is consistent with phosphosite distributions previously reported for
265 Arabidopsis (Champion et al., 2004; Sugiyama et al., 2008). The phosphosite residue distributions
266 were similar at ZT14 (**Figure 3A**).

267 We performed *mlk*-to-WT pairwise comparisons for each time point (**Supplemental Table S1 and**
268 **Dataset S2**) to identify peptides that showed altered phosphorylation in the absence of the MLKs
269 at either ZT12 or ZT14. Peptides were considered differentially phosphorylated if they had a
270 minimum $\log_2$ FC of ±0.585 (1.5 fold-change) and a p-value < 0.05. We identified 113
271 phosphopeptides corresponding to 93 unique protein groups that met the cutoff in the *mlk1/2/3*
272 ZT12 set. In the *mlk1/3/4* ZT12 set, 429 phosphopeptides corresponding to 284 unique proteins
273 showing differential phosphorylation were identified, which corresponds to a 300% increase (**Fig.**
274 **3B**). 170 and 274 phosphopeptides, corresponding to 149 and 215 unique protein groups, have
275 altered phosphorylation in the *mlk1/2/3* ZT14 and *mlk1/3/4* ZT14 analysis, respectively (**Figure.**
276 **3B and Supplemental Table S1**). The phosphosite residue distribution was similar in all datasets
277 analyzed (**Figure 3A**). These data show that the *mlk1/3/4* mutant combination has a larger impact
278 on the phosphoproteome than the *mlk1/2/3* mutant combination at each time point, particularly at
279 ZT12. This observation supports a role for MLK4 in regulating the phosphoproteome in a light-
280 dependent manner, which is in agreement with the known role of MLK4 in phosphorylating key
281 components of blue- and red-light signaling pathways (Liu et al., 2017; Ni et al., 2017).

282 Over 50% (48 out of 93) of the differentially phosphorylated proteins identified in the *mlk1/2/3*
283 ZT12 set were also identified in the *mlk1/3/4* ZT12 set. In contrast, over 80% of those identified
284 in the *mlk1/3/4* ZT12 set were specific to the *mlk1/3/4* mutant (**Fig. 3C**). When comparing the
285 ZT14 sets, 42 phosphoproteins were shared, accounting for 28% and 19.5% of the proteins
286 identified in the *mlk1/2/3* ZT14 and *mlk1/3/4* ZT14 sets, respectively (**Fig. 3D**). Many of the
287 proteins shared between *mlk1/2/3* and *mlk1/3/4* protein sets are involved in gene silencing and
288 chromatin organization (**Supplemental Dataset S2**), supporting a conserved role for the MLK
289 family kinases in these processes (Casas-Mollano et al., 2008; Jeong Br et al., 2002). Some of
290 these proteins, including SUO and SERRATE (SE) – which are involved in microRNA biogenesis
291 pathways, exhibit altered phosphopeptide abundance at both ZT12 and ZT14. However, proteins

292 involved in chromatin organization, such as Increased in Bonsai Methylation 1 (IBM1) and
293 SPLAYED (SYD), only showed altered phosphorylation in both *mlk1/2/3* and *mlk1/3/4* mutant
294 backgrounds at ZT12 (**Supplemental Dataset S2**). These results suggest that the MLKs are
295 involved in regulating gene expression, possibly through modulating light-dependent chromatin
296 organization.

297 **MLKs Influence Diverse Kinase Signaling Networks**

298 The proteins identified as differentially phosphorylated in the *mlk1/3/4* mutant background at both
299 ZT12 and ZT14 are associated with a diverse set of biological processes, suggesting a possible
300 disruption of multiple protein kinase networks. Motif-X (http://motif-x.med.harvard.edu/motif-
301 x.html; (Chou and Schwartz, 2011; Schwartz and Gygi, 2005) was used to isolate
302 overrepresented sequence motifs present in the phosphopeptide sets that are associated with
303 known kinase families. Following extension of differentially phosphorylated high-confidence,
304 unambiguous peptides using PEPTIDEXTENDER ver.0.2.2 alpha
305 (http://schwartzlab.uconn.edu/pepextend), the resulting 15-mers were submitted for motif
306 analysis using a significance threshold of $p < 10^{-6}$ and a minimum occurrence requirement of 20.
307 Peptides exhibiting increased or decreased abundance when compared to wild type were
308 analyzed separately. Three serine phosphorylation (Sp) motifs (S-x-x-K, R-x-x-S, and K-x-x-S)
309 were found to be overrepresented in peptides that were decreased in abundance at ZT12 in the
310 *mlk1/3/4* mutant seedling background (**Fig. 4A**). The K-x-x-S motif, along with an acidic S-type
311 motif (S-x-x-x-x-x-E), was also found to be overrepresented at ZT14 in *mlk1/3/4* mutants (**Fig.
312 4B**). The CDPK-SnRK superfamily of protein kinases is known to recognize R/K-x-x-S/T basic
313 motifs. The R-x-x-S motif has also been associated with the AGC family kinases, PKA and PKC
314 (Rademacher and Offringa, 2012; Marondedze et al., 2016), which are involved in mid- to late-
315 day rhythmic phosphorylation (Choudhary et al., 2015). The kinase(s) responsible for
316 phosphorylation at the S-x-x-K site in plants is less well-characterized. However, it was recently

317 shown that the highly conserved eukaryotic cyclin B-dependent protein kinase Cdk1 recognizes
318 several non-S/T-P motifs including the S/T-x-x-R/K motif (Suzuki et al., 2015). The classical
319 minimal motif required for recognition by proline-directed kinases families (mitogen-activated
320 protein kinase (MAPK), cyclin-dependent kinase (CDK), and glycogen synthase kinase 3 (GSK-
321 3)), S-P, was found to be overrepresented in peptides that were increased in abundance in
322 *mlk1/3/4* mutants at ZT12 and ZT14. While the S-x-S motif, which is associated with the receptor-
323 like protein kinase (RLK) family (van Wijk et al., 2014), was only found to be overrepresented at
324 ZT12 (**Fig. 4**). Using the same parameters, there were no overrepresented motifs identified from
325 the sites that decreased in abundance in neither of the *mlk1/2/3* data sets. However, if the
326 minimum occurrence was reduced to 10, the R-x-x-S and S-P motifs were found to be
327 overrepresented in peptides with decreased or increased abundance at ZT12 in *mlk1/2/3* mutants
328 (**Supplemental Figure S2**)**.** The diversity of identified overrepresented kinases motifs suggests
329 that MLK family kinases influence numerous biological processes through systemic regulation of
330 multiple kinase signaling networks.

331 **MLKs May Regulate Glucosinolate Metabolism**

332 *In silico* classification using Gene Ontology (GO) analysis (https://biit.cs.ut.ee/gprofiler/) revealed
333 that proteins exhibiting altered abundance were associated with biotic and abiotic stresses (**Fig.**
334 **5**). To simplify the enriched GO term lists and focus on the most relevant terms, we performed
335 additional analysis using REVIGO (default settings, dispensability threshold = 0.7) to remove
336 functionally redundant terms (Supek et al., 2011). Proteins involved in glucosinolate biosynthesis
337 (GO:0019761) and related processes (GO:1901659, GO:0016143, and GO:0044272) were found
338 to have increased abundance in *mlk1/3/4* mutant seedlings at ZT12 and in both *mlk1/2/3* and
339 *mlk1/3/4* mutant seedlings at ZT14 (**Fig. 5**). Nearly 75% of the peptides with an increased
340 abundance of 3-fold or greater in the *mlk1/3/4* mutant seedlings at ZT14 mapped to proteins
341 directly involved in glucosinolate biosynthesis (**Supplemental Dataset S1**). These proteins

342 include enzymes responsible for the early reactions leading to methionine-derived glucosinolates
343 (branched-chain aminotransferase 4 (BCAT4) and methylthioalkymalate synthase 1 (MAM1)) as
344 well as, desulfo-glucosinolate sulfotransferase 17 and 18 (SOT17 and SOT18), which are
345 involved in the final step of glucosinolate core structure biosynthesis (Sønderby et al., 2010).
346 Other proteins involved in glucosinolate biosynthesis that showed increased abundance in
347 *mlk1/3/4* mutants compared to wild type include isopropymalate dehydrogenase 1 (IMD1),
348 iospropylmaate isomerase 2 (IPMI2), 2-isopropylmalate synthase 2 (IMS2), flavin-
349 monooxygenase glucosinolate S-oxygenase 1 (FMO GS-OX1) and the cytochrome P_{450} proteins
350 CYP83A1 and CYP79F1 (**Supplemental Dataset S1**). Proteins involved in glucosinolate
351 catabolism such as glucoside glucohydrolase 2 (TGG2), nitrile specifier protein 1 (NSP1), and
352 beta glucosidase 34 and 35 (BGLU34 and BGLU35) were decreased in abundance in *mlk1/3/4*
353 mutant seedlings at ZT12 compared to wild type.

354 To begin testing the hypothesis that MLKs are involved in the regulation of glucosinolate
355 metabolism, we quantified glucosinolate levels at the end of day (ZT12) when GLS levels are
356 expected to peak (Huseby et al., 2013). Total GLSs were extracted from whole seedlings and
357 analyzed by HPLC. Peaks corresponding to individual GLSs were identified by comparison with
358 published UV absorbance spectra and expected retention times and the identities were validated
359 using LbyC-MS/MS. These analyses revealed an increase in aliphatic glucosinolates (Met-
360 derived) in both *mlk1/2/3* and *mlk1/3/4* mutant seedlings compared to wild type, whereas the
361 levels of indolic glucosinolates (Trp-derived) remained unchanged in the mutant backgrounds
362 (**Fig. 6**). Interestingly, the first seven glucosinolates originating from the earliest steps in the Met-
363 derived glucosinolate biosynthetic pathway were increase 2- to 4-fold over wild type (**Fig. 6**), a
364 pattern which correlates with the increased abundance of glucosinolate-associated biosynthetic
365 enzymes (BCAT4, MAM1, SOT17/18, etc.) in the *mlk* mutants. Together these findings support a

366 role for the MLKs in early stages of aliphatic glucosinolate biosynthesis and overall glucosinolate
367 metabolism.

368 In addition to glucosinolate biosynthetic enzymes, several proteins involved in hormone signaling
369 and diverse stress responses exhibited differential abundance in *mlk1/3/4* mutant seedlings
370 compared to wild type at either ZT12 or ZT14, including BRI1-EMS-SUPPRESSOR 1 (BES1),
371 SUPER SENSITIVE TO ABA AND DROUGHT2 (SAD2), CORONATINE INDUCED 1 (CORI3),
372 pathogenesis-related gene 5 (PR5), lipoxygenase 2 (LOX2), thylakoidal ascorbate peroxidase
373 (TAPX), and cold regulated 15a and b (COR15A and COR15B). Peptides mapping to the blue
374 light receptor cryptochrome 2 (CRY2) also showed an increased abundance of 2-fold in the
375 *mlk1/3/4* mutant when compared to wild type at ZT12 (**Supplemental Dataset 1**). These
376 observations are in agreement with the previously reported role of MLKs in hormone signaling,
377 stress response, and light signaling (Liu et al., 2017; Dai and Xue, 2010; Casas-Mollano et al.,
378 2008; Ni et al., 2017; Chen et al., 2018).

379 **MLKs Influence the Phosphorylation Status of Nuclear Localized Proteins**

380 Using g:Profiler (https://biit.cs.ut.ee/gprofiler/), 149 GO terms were found to be enriched in the
381 differentially phosphorylated proteins from the *mlk1/3/4 Z*T12 set; 107 of these were classified as
382 biological process, 34 as cellular component, and 5 as molecular function. Forty-nine terms were
383 found to be enriched in the *mlk1/3/4 Z*T14 set, 28 biological process and 21 cellular components.
384 Fewer terms were found to be enriched in the *mlk1/2/3* phosphoprotein sets, with only 8 enriched
385 terms at ZT12 and 18 at ZT14. A complete list of enriched GO terms can be found in
386 **Supplemental Dataset S2**. Functionally redundant terms were removed using REVIGO (default
387 settings, dispensability threshold = 0.7 (cellular component) or 0.5 (biological process);
388 **Supplemental Tables S2-3;** (Supek et al., 2011)). Under the cellular component category, there
389 was strong enrichment for terms associated with the nucleus: 'nucleus' (GO:0005634), 'nuclear
390 part' (GO:0044428), and 'nucleoplasm' (GO:0005654). Terms including 'chromosome'

391 (GO:0005694), ‘chromosomal part’ (GO:0044427) and ‘chromatin’ (GO:0000785) were also found
392 to be enriched in at least one of the differentially phosphorylated protein lists (**Fig. 7A**). These
393 results are in agreement with the known nuclear localization of the MLKs, and their role in
394 modifying chromatin (Wang et al., 2015a; Huang et al., 2016; Su et al., 2017).

395 **Circadian-Associated Proteins Exhibit Altered Phosphorylation in *mlk1/3/4* Mutant**
396 **Seedlings**

397 The *mlk1/3/4* ZT12 differentially phosphorylated protein set was enriched in proteins associated
398 with rhythmic processes (GO:0048511) and/or circadian rhythms (GO:0007623). These
399 observations agree with previous reports linking the MLKs to light signaling and circadian
400 regulation (Huang et al., 2016; Ni et al., 2017; Liu et al., 2017; Su et al., 2017; Zheng et al., 2017).
401 The core circadian clock proteins PSEUDO-RESPONSE REGULATOR 7 (PRR7), TIME FOR
402 COFFE (TIC), and REVEILLE 8 (RVE8) were all differentially phosphorylated in the *mlk1/3/4*
403 mutant background at ZT12 (**Table 1 and Supplemental Table S3**). We observed decreased
404 phosphorylation of TIC at S324 and PRR7 at S355 and S275, while RVE8 showed increased
405 phosphorylation of the C-terminal half (**Table 1**). The red-light photoreceptor phytochrome B
406 (PHYB) and the transcriptional master regulator ELONGATED HYPOCOTYL 5 (HY5) also
407 showed reduced phosphorylation at Threonine 42 and T64, respectively (**Table 1**); to the best of
408 our knowledge, these phosphosites are previously unreported. A complete list of circadian-
409 associated proteins with altered phospho-abundance in the *mlk1/3/4* mutant at ZT12 can be found
410 in **Table 1**.

411 **Gene Ontology Analysis Reveals Enrichment of Proteins Involved in Chromatin**
412 **Organization**

413 Due to the large number of enriched GO terms identified from both the *mlk1/3/4 Z*T12 and
414 *mlk1/3/4 Z*T14 list, the dispensability threshold was reduced to 0.5 for REVIGO analysis. This

415 resulted in the identification of 34 and 15 representative and non-redundant enriched biological
416 process terms in *mlk1/3/*4 ZT12 and *mlk1/3/4 Z*T14 altered phosphoprotein lists, respectively.
417 Many of the enriched GO terms and their underlying gene identifiers were shared between the
418 *mlk1/3/4 Z*T12 and ZT14 sets including, 'organic cyclic compound metabolism', GO:1901360,
419 'nitrogen compound metabolism', GO:0006807, 'chromosome organization', GO:0051276 and
420 'negative regulation of gene expression' GO:0006807 (**Fig. 7B-C and Supplemental Table S3**).
421 The chromatin modifying proteins BRAHMA (BRM), SIN3-like3 (SNL3), vernalization5/VIN3-like
422 (VEL1), and high mobility ground B1 (HMGB1) were shared amongst these GO terms. Additional
423 proteins associated with chromatin modifications were present in the *mlk1/3/4 Z*T12 list including
424 the histone methyltransferase EARLY FLOWERING IN SHORT DAYS (EFS)/SET DOMAIN
425 GROUP 8 (SDG8), the histone acetyltransferase TBP-ASSOCIATED FACTOR 1 (TAF1), as well
426 as IBM1, actin-related protein 4 (ARP4), alfin-like 7 (AL7), GLIOMAS 41 (GAS41/YAF9a), and
427 stress-induced histone H2A protein 9 (HTA9). Few biological process GO-terms were found to be
428 enriched in the *mlk1/2/3* data sets, but those that were ('regulation of gene expression',
429 'epigenetic' (ZT12) and 'chromosome organization', 'chromatin organization' and 'mitotic sister
430 chromatid cohesion' (ZT14)) were also found to be enriched in the *mlk1/3/4* protein list
431 (**Supplemental Dataset S2**). These results support a role for the MLKs in regulating chromatin
432 organization and gene expression at the assessed time points.

433 ***mlk1/3/4* Mutants Show Altered Phosphorylation of Proteins Involved in Nuclear**
434 **Organization and DNA Damage Response**

435 Our analysis of differentially phosphorylated peptides has shown that the loss of functional
436 versions of *mlk1*, *mlk3*, and *mlk4* at ZT12 has the greatest impact on both the global- and
437 phospho- proteomes. Therefore, we chose to expand on our analysis exclusively for the *mlk1/3/4*
438 ZT12 data set. The phosphoproteins that were increased or decreased in abundance
439 independently were analyzed to further elucidate biological processes influenced by the MLKs at

440 the end of the day (ZT12). Of the 429 phosphopeptides found to have altered abundance in the
441 *mlk1/3/4* mutant background at ZT12 (**Supplemental Dataset S2**), 133 were increased and 296
442 were decreased in abundance, mapping to 103 increased and 190 decreased unique proteins.
443 Interestingly, 9 gene identifiers were shared between the increased and decreased groups,
444 including several that are involved in various aspects of nuclear organization such as LITTLE
445 NUCLEI 1/ CROWED NUCLEI 1 (LINC1/CRWN1), VEL1, and HMGB1 (**Fig. 8A and**
446 **Supplemental Dataset 2**). Proteins that were increased in abundance were associated with the
447 representative GO-terms 'response to organic substance' (GO:0010033) and 'response to
448 stimulus' (GO:0050896) (**Fig. 8B**). However, we found that the majority of GO terms enriched in
449 the inclusive set (both increased and decreased peptides) such as 'RNA processing'
450 (GO:0006396), 'chromosome organization' (GO:0051276), and 'developmental processes'
451 (GO:0032592) are associated with decreased phosphorylation (**Fig. 8C**). The GO term 'cellular
452 response to DNA damage stimulus' (GO:0006974), was also found to be enriched in proteins
453 exhibiting decreased phosphorylation. Proteins associated with this term include a catalytic
454 subunit of DNA polymerase alpha INCARVATA2 (ICU2), as well as X-ray cross complementation
455 group4 (XRCC4) and MUTM homolog-1 (MMH-1) both of which are directly involved in DNA repair
456 (West et al., 2000; Ohtsubo et al., 1998; Barrero et al., 2007).

457 ***mlk* Mutants Show Increased Sensitivity to DNA-damaging Agents**

458 It is well established that nuclear organization and chromatin dynamics strongly influence DNA
459 damage repair efficacy (Reviewed in Vergara and Gutierrez, 2017; Donà and Mittelsten Scheid,
460 2015). Additionally, it has been previously shown that the *Chlamydomonas* MLK orthologue,
461 Mut9, is required for survival when grown in the presence of genotoxic agents (Jeong Br et al.,
462 2002). Since many of the proteins associated with changes in phosphorylation abundance in the
463 *mlk1/3/4* mutants at ZT12 are proteins associated with nuclear organization (LINC/CRWN family
464 members, SAD1/UNC-84 domain protein 2 (SUN2), BRM, and SYD) and DNA damage, we

465 sought to further explore what role the *Arabidopsis* MLKs might play in DNA damage response.
466 To do so, we evaluated the sensitivity of mutant and wild type seedlings to the genotoxic agent
467 methyl methane sulfonate (MMS) and UV-C. MMS is a monofunctional DNA alkylating agent
468 which induces replication fork stalling and subsequent double strand breaks (Ensminger et al.,
469 2014). In addition to the *mlk1/2/3* and *mlk1/3/4* mutants, the *mlk4* single and *mlk* quadruple
470 amiRNA line (amiR^{4k})(Liu et al., 2017) were included in our analysis. Five days after germination,
471 mutant and wild type seedlings were transferred to solid media containing increasing levels of
472 MMS and allowed to grow for an additional 14 days, after which point seedlings were imaged and
473 weighed (**Fig. 9A-B**). After 2 weeks of treatment, all genotypes showed a reduction in aerial mass
474 correlating with increasing levels of MMS. This reduction was greater in *mlk* mutants compared
475 to wild-type seedlings, which exhibited a less than 10% reduction in fresh weight (FW) when
476 grown in the presence of 50 ppm MMS compared to the mock treated seedlings. The *mlk4* single
477 mutant seedlings had a more than 20% reduction of FW compared to the mock treated seedlings.
478 The reductions were even greater in the *mlk1/3/4* and amiR^{4K} lines, with a FW of 61% and 56%
479 of mock treated seedlings, respectively (**Fig. 9B**). The *mlk1/3/4* and amiR^{4k} mutants continued to
480 show greater reduction of FW than wild type in all concentration tested. At 100 ppm MMS,
481 *mlk1/2/3* seedlings showed approximately a 10% greater reduction in FW than what was observed
482 for wild type (i.e. 49% and 61%, respectively, **Fig. 9B**). In addition to overall growth reduction, the
483 appearance of chlorotic tissue was observed in the *mlk134* mutants growing on as little as 50 ppm
484 MMS and in the amiR^{4K} mutants at 75 PPM MMS (**Fig. 9A**). Growth in the presence of 150 ppm
485 MMS caused severe growth reduction and lethality in all post-germination growth development in
486 the presence of 150 ppm MMS genotypes assessed, thus seedlings were imaged but not
487 weighted (**Fig. 9A**). Post-germination growth was found to be severely impaired in the *mlk1/3/4*
488 mutant, with more than 65% of seedlings exhibiting complete developmental arrest compared to
489 approximately 10% in wild-type seedlings (**Fig. 9C-D**). The *amiR^{4k}* mutant seedlings developed
490 similar to wild-type seedlings when germinated in the presence of 150 ppm MMS (**Fig. 9C-D**),

491 which could be a result of near endogenous expression levels of MLK2 and MLK3 (Ni 2017).
492 Sensitivity to UV-induced DNA damage was also assessed after periodic exposure to multiple
493 doses of UV-C irradiation. The phenotypic impact of chronic irradiation with either 2000 or 4000
494 J m^{-2} on seedlings was evaluated 5 days after a recovery period. Cotyledon cell death and
495 reduced growth was observed in all genotypes after exposure to both doses of UV-C. However,
496 tissue chlorosis was only observed in *mlk1/3/4* mutant seedlings after exposure to 2000 and 4000
497 J m^{-2}. Minimal chlorosis was also observed in the amiR^{4k} mutants after irradiation with 4000 J m^{-}
498 ^{2} (**Fig. 9E**). Taken together, these data suggest that *mlk* mutants have increased sensitivity to
499 DNA damage.

500 **Discussion**

501 **MLK protein kinases alter developmental and stress response pathway protein**
502 **phosphorylation**

503 The current repertoire of MLK and MLK homologue substrates is composed of a photoreceptor,
504 multiple transcription factors, hormone receptors, and histones (Ni et al., 2017; Liu et al., 2017;
505 Dai and Xue, 2010; Chen et al., 2018; Casas-Mollano et al., 2008; Su et al., 2017). In the absence
506 of the MLKs, effects on circadian period, hypocotyl elongation, flowering time, osmotic stress
507 response, seed set, chromatin organization, and hormone sensitivity have been reported (Su et
508 al., 2017; Casas-Mollano et al., 2008; Liu et al., 2017; Huang et al., 2016; Zheng et al., 2017;
509 Chen et al., 2018). These observations support a model where MLK family members function as
510 central regulators of numerous interconnected signaling pathways. Our quantitative analysis of
511 the global- and phosphoproteomes of *mlk* triple mutant seedlings supports a diverse and complex
512 role for the MLKs in the regulation of cellular signaling and response. Interestingly, these kinases
513 seem to share a balance of functional redundancy and substrate specificity which, with respect to
514 circadian period and hypocotyl elongation, results in opposing phenotypes (Huang et al., 2016;
515 Liu et al., 2017). We found *mlk4* the *mlk134* mutant displays a much more severe proteomic

516 phenotype relative to the *mlk123* mutant, with over 10-fold more proteins showing altered
517 abundance in the *mlk134* mutant (**Fig. 2**). This holds true for the phosphoproteome as well.
518 However, the difference was greater in tissue sampled in the light. This could be the result of
519 MLK4 acquiring substrate specificity or may be explained by MLK4 having a greater tendency
520 than other MLKs for interacting with key light signaling proteins in planta. MLK4 has been shown
521 to have a higher affinity for PIF3, a known substrate of MLK4, when compared to other MLKs (Ni
522 et al., 2017) and both phyB and HY5 were found to have altered phosphorylation only at ZT12 in
523 the *mlk134* mutants (**Table 1**). While some proteins with altered abundance were unique to the
524 *mlk134* or *mlk123* mutants, the common themes of glucosinolate biosynthesis (global proteome;
525 **Fig. 3**) and chromosome organization (phosphoproteome; **Fig. 7B-C and Supplemental Dataset**
526 **S2**) are seen in both mutants, suggesting a role for the MLK family of kinases in these processes.
527 Further work is needed to determine if any of the proteins showing altered phosphorylation are
528 direct substrates of the MLKs, or whether changes in phosphorylation status is occurring indirectly
529 through additional kinases.

530 **MLKs Regulate Hormone Signaling and Stress Responses**

531 Several proteins responsible for glucosinolate metabolism showed altered abundance in *mlk*
532 mutant seedlings before and after dark transition (**Fig. 3** and **Supplemental Dataset S1**).
533 Glucosinolates are nitrogen- and sulfur-containing secondary metabolites known for their role in
534 plant defense (Kim et al., 2008; Kos et al., 2012; Bednarek et al., 2009; Clay et al., 2009) and for
535 their anticarcinogenic properties (Higdon et al., 2007). Accumulation of glucosinolates in
536 *Arabidopsis thaliana* is a rhythmic process controlled in part by circadian-regulated jasmonate
537 accumulation that has been linked to the activity of the basic leucine zipper (bZIP) transcription
538 factor, ELONGATED HYPOCOTYL 5 (HY5) activity (Goodspeed et al., 2012; Huseby et al.,
539 2013). HY5 is a positive regulator of light signaling and functions as a central regulator of light-
540 dependent growth and development by integrating various environmental signals (Gangappa and

541 Botto, 2016). Peak glucosinolate levels occur during the day, which may provide a protective
542 advantage against rhythmic herbivory. Two glucosinolate biosynthesis genes that showed
543 increased protein abundance in *mlk* mutants, *CYP79F1* and *SOT18*, showed reduced expression
544 in the hy5 mutant background (Huseby et al., 2013). The phosphorylation-status of HY5 is
545 associated with its activity and stability, with the non-phosphorylated form being more active
546 (Hardtke, 2000). Thus, it is possible that increased HY5 activity, resulting from decreased
547 phosphorylation in the *mlk* mutant background, could be influencing glucosinolate metabolism.
548 Additionally, abscisic acid (ABA) is capable of inducing glucosinolate accumulation in plants
549 (Wang et al., 2015b; Zhu and Assmann, 2017). MLK3 has been shown to regulate ABA signaling
550 through the phosphorylation of the PYR/PYL ABA receptor family of proteins (Chen et al., 2018).
551 In agreement with altered ABA signaling, increased phosphorylation of proteins associated with
552 ABA responses and the SnRK consensus motif, R/K-x-x-S/T, was found to overrepresented in
553 the *mlk1/3/*4 mutant background. Thus, it is possible that the MLKs are involved in the regulation
554 of defense responses through multiple converging signaling pathways.

555 **The Phosphorylation Status of Key Circadian and Light Signaling Components Are Altered**
556 **in the Absence of MLK Family Kinases**

557 Several differentially phosphorylated proteins that are involved in chromatin organization also
558 function as core circadian clock components (RVE8) or are central regulators of clock input
559 pathways such as temperature and light signaling (phyB and HY5). RVE8 is a MYB-like
560 transcription factor that regulates the expression of the clock gene TIMING OF CAB
561 EXPRESSION1 (TOC1) by promoting histone 3 (H3) acetylation of its promoter (Farinas and Mas,
562 2011). RVE8 shares structural similarity to the core clock transcription factors CCA1 and LATE
563 ELONGATED HYPOCOTYL (LHY). Phosphorylation of CCA1 by the Ser/Thr protein kinase CK2
564 antagonistically regulates CCA1 transcriptional activity by reducing its ability to bind to the
565 promoters of clock gene targets, which in turn alters circadian period (Portolés and Más, 2010).

566 Further exploration of the impact of RVE8 phosphorylation could reveal a new avenue of post-
567 translation regulation of the circadian clock.

568 Temperature and light signaling are critical circadian inputs that allow plants to coordinate growth
569 and development (*e.g.* germination and photoperiodic flowering) with their environment. The phyB
570 photoreceptor is central to both temperature and light signaling pathways (Legris et al., 2016).
571 PhyB activity is regulated in part by phosphorylation of its N-terminus (Medzihradszky et al., 2013;
572 Nito et al., 2013). Altered phospho-status of phyB Ser86 and Y10 influences phyB rate dark-
573 reversion rates, hypocotyl elongation, and flowering time in Arabidopsis (Hajdu et al., 2015;
574 Medzihradszky et al., 2013; Nito et al., 2013). Here we report decreased phosphorylation of a
575 previously unidentified phyB N-terminal phosphosite, T42, in the *mlk* mutant background at ZT12
576 (**Table 2**). MLKs are known to associate with phyB, phosphorylate the phytochrome–interacting
577 factor, PIF3, and display a variety of red-light dependent growth phenotypes (Ni et al., 2017;
578 Huang et al., 2016). In addition to the well-established light-induced phyB-PIF signaling cascade,
579 there is an ample amount of evidence supporting the role of phyB in large-scale chromatin
580 organization (van Zanten et al., 2010; Tessadori et al., 2009). The MLK-phyB interaction may
581 contribute to light-dependent chromatin re-organization in addition to regulating PIF3 turnover.
582 We also found decreased phosphorylation in another key light signaling component, HY5 at T64.
583 Whether the phosphorylation of $HY5^{T64}$ and/or $phyB^{T42}$ is directly or indirectly influenced by the
584 MLKs and how those phosphosites fit into the existing light signaling paradigm will be an exciting
585 line of future research.

586 **The Role of MLK Family Kinases in Modulating Nuclear Architecture**

587 The role of histone modifications in the regulation of developmental processes and stress
588 response has been well-established, yet our understanding of the responsible modifiers,
589 modification crosstalk, and targeted genes is incomplete (Probst and Mittelsten Scheid, 2015;
590 Rosa and Shaw, 2013). Early observations have implicated the MLK family in the regulation of

591 environmentally-stimulated chromatin organization. MLK1, like its *Chlamydomonas* homologue
592 MUT9, has been shown to phosphorylate histone H3 on threonine 3 (H3T3p) and to function
593 redundantly with MLK2 to promote H3T3p in response to salt stress (Wang et al., 2015a; Casas-
594 Mollano et al., 2008). Accordingly, the *mlk1mlk2* double mutant has abnormal chromatin
595 organization and an increased sensitivity to osmotic stress (Wang et al., 2015a). Comparisons
596 have been drawn between the defects in chromosomal organization observed in the *mlk1mlk2*
597 mutants and those occurring in plants harboring mutations in members of the LITTLE
598 NUCLEI/CROWDED NUCLEI (LINC/CRWN) gene family, which are involved in controlling
599 nuclear size and heterochromatin organization (Wang et al., 2013; Sakamoto and Takagi, 2013).
600 Our analysis of the *mlk* mutant phosphoproteomes found that peptides mapping to multiple
601 members of the LINC/CRWN family were altered in abundance in *mlk123* and *mlk134* mutants,
602 suggesting that MLKs may influence nuclear organization in part through regulation of the LINC
603 proteins.

604 **MLKs Are Involved in May Influence DNA Damage Repair Through Multiple Pathways**

605 Plants are continuously subjected to DNA-damage from their external environment (e.g. ultraviolet
606 light, ionizing radiation, heat stress, and bacterial and fungal toxins) as well as endogenous
607 sources such as DNA-alkylating metabolic byproducts. Maintenance of genomic integrity requires
608 an efficient DNA damage repair (DDR) system that can identify, access, remove and reassemble
609 damaged genomic regions and requires fluidity within the context of chromatin. Mutations in
610 genes involved in chromatin organization and remodeling often exhibit defects in DDR and
611 enhanced susceptibility to DNA damaging reagents (Donà and Mittelsten Scheid, 2015).
612 Dysregulation of proteins involved in chromatin remodeling such as GAS41/YAFa, ARP4, BRM,
613 and SYD which we have observed (*vida supra*) is one route by which the increased sensitivity of
614 *mlk* mutants to DNA damaging agents (**Fig. 9**) can be explained. The *mlk134* mutant also shows
615 altered phosphorylation of several proteins directly involved in DDR such as MMH-1 and XRCC4

616 (Yuan et al., 2014; Roy et al., 2013). Additionally, there is accumulating evidence supporting a
617 role for small regulatory RNAs in DDR (Hawley et al., 2017); proteins associated with small RNA
618 metabolism are enriched in *mlk134* at ZT12 (**Fig. 7**). There is no question that full elucidation and
619 validation of the mechanisms linking MLKs and DDR will require further exploration. However,
620 taken together, our data suggests the MLKs play an important role in mitigating DNA damage
621 through regulation of multiple response pathways.

622

623

624

625

626

627

628

629

630

631

632

633

634

635

636

637 **References**

638 **Barrero, J.M., Gonzalez-Bayon, R., del Pozo, J.C., Ponce, M.R., and Micol, J.L.** (2007).
639 INCURVATA2 Encodes the Catalytic Subunit of DNA Polymerase and Interacts with
640 Genes Involved in Chromatin-Mediated Cellular Memory in Arabidopsis thaliana. PLANT
641 CELL ONLINE.

642 **Bednarek, P., Piślewska-Bednarek, M., Svatoš, A., Schneider, B., Doubský, J.,**
643 **Mansurova, M., Humphry, M., Consonni, C., Panstruga, R., Sanchez-Vallet, A.,**
644 **Molina, A., and Schulze-Lefert, P.** (2009). A Glucosinolate Metabolism Pathway in Living
645 Plant Cells Mediates Broad-Spectrum Antifungal Defense. Science (80-.). **323**: 101 LP –
646 106.

647 **Casas-Mollano, J.A., Jeong, B.-R., Xu, J., Moriyama, H., and Cerutti, H.** (2008). The MUT9p
648 kinase phosphorylates histone H3 threonine 3 and is necessary for heritable epigenetic
649 silencing in Chlamydomonas. Proc. Natl. Acad. Sci. U. S. A.

650 **Champion, A., Kreis, M., Mockaitis, K., Picaud, A., and Henry, Y.** (2004). Arabidopsis
651 kinome: After the casting. Funct. Integr. Genomics.

652 **Chen, H.-H., Qu, L., Xu, Z.-H., Zhu, J.-K., and Xue, H.-W.** (2018). EL1-like Casein Kinases
653 Suppress ABA Signaling and Responses by Phosphorylating and Destabilizing the ABA
654 Receptors PYR/PYLs in Arabidopsis. Mol. Plant **11**: 706–719.

655 **Chou, M.F. and Schwartz, D.** (2011). Biological sequence motif discovery using motif-x. Curr
656 Protoc Bioinforma.

657 **Choudhary, M.K., Nomura, Y., Wang, L., Nakagami, H., and Somers, D.E.** (2015).
658 Quantitative Circadian Phosphoproteomic Analysis of Arabidopsis Reveals Extensive Clock
659 Control of Key Components in Physiological, Metabolic, and Signaling Pathways. Mol. Cell.

660 Proteomics.

661 **Clay, N.K., Adio, A.M., Denoux, C., Jander, G., and Ausubel, F.M.** (2009). Glucosinolate
662 metabolites required for an Arabidopsis innate immune response. Science (80-.).

663 **Dai, C. and Xue, H.W.** (2010). Rice early flowering1, a CKI, phosphorylates della protein SLR1
664 to negatively regulate gibberellin signalling. EMBO J.

665 **Donà, M. and Mittelsten Scheid, O.** (2015). DNA Damage Repair in the Context of Plant
666 Chromatin. Plant Physiol.

667 **Ensminger, M., Iloff, L., Ebel, C., Nikolova, T., Kaina, B., and Löbrich, M.** (2014). DNA
668 breaks and chromosomal aberrations arise when replication meets base excision repair. J.
669 Cell Biol.

670 **Farinas, B. and Mas, P.** (2011). Functional implication of the MYB transcription factor
671 RVE8/LCL5 in the circadian control of histone acetylation. Plant J.

672 **Gangappa, S.N. and Botto, J.F.** (2016). The Multifaceted Roles of HY5 in Plant Growth and
673 Development. Mol. Plant.

674 **Goodspeed, D., Chehab, E.W., Min-Venditti, A., Braam, J., and Covington, M.F.** (2012).
675 Cozzarelli Prize Winner: Arabidopsis synchronizes jasmonate-mediated defense with
676 insect circadian behavior. Proc. Natl. Acad. Sci.

677 **Hajdu, A., Ádám, É., Sheerin, D.J., Dobos, O., Bernula, P., Hiltbrunner, A., Kozma-Bognár,**
678 **L., and Nagy, F.** (2015). High-level expression and phosphorylation of phytochrome B
679 modulates flowering time in Arabidopsis. Plant J.

680 **Hardtke, C.S.** (2000). HY5 stability and activity in Arabidopsis is regulated by phosphorylation in
681 its COP1 binding domain. EMBO J.

682 **Hawley, B.R., Lu, W.-T., Wilczynska, A., and Bushell, M.** (2017). The emerging role of RNAs
683 in DNA damage repair. Cell Death Differ.

684 **Higdon, J. V., Delage, B., Williams, D.E., and Dashwood, R.H.** (2007). Cruciferous
685 vegetables and human cancer risk: epidemiologic evidence and mechanistic basis.
686 Pharmacol. Res.

687 **Huang, H., Alvarez, S., Bindbeutel, R., Shen, Z., Naldrett, M.J., Evans, B.S., Briggs, S.P.,**
688 **Hicks, L.M., Kay, S.A., and Nusinow, D.A.** (2016). Identification of evening complex
689 associated proteins in arabidopsis by affinity purification and mass spectrometry. Mol. Cell.
690 Proteomics.

691 **Huseby, S., Koprivova, A., Lee, B.R., Saha, S., Mithen, R., Wold, A.B., Bengtsson, G.B.,**
692 **and Kopriva, S.** (2013). Diurnal and light regulation of sulphur assimilation and
693 glucosinolate biosynthesis in Arabidopsis. J. Exp. Bot.

694 **Jeong Br, B., Wu-Scharf, D., Zhang, C., and Cerutti, H.** (2002). Suppressors of transcriptional
695 transgenic silencing in Chlamydomonas are sensitive to DNA-damaging agents and
696 reactivate transposable elements. Proc. Natl. Acad. Sci. U. S. A.

697 **Kim, J.H., Lee, B.W., Schroeder, F.C., and Jander, G.** (2008). Identification of indole
698 glucosinolate breakdown products with antifeedant effects on Myzus persicae (green
699 peach aphid). Plant J.

700 **Kos, M., Houshyani, B., Achhami, B.B., Wietsma, R., Gols, R., Weldegergis, B.T., Kabouw,**
701 **P., Bouwmeester, H.J., Vet, L.E.M., Dicke, M., and van Loon, J.J.A.** (2012). Herbivore-
702 Mediated Effects of Glucosinolates on Different Natural Enemies of a Specialist Aphid. J.
703 Chem. Ecol.

704 **Legris, M., Klose, C., Burgie, E.S., Rojas, C.C., Neme, M., Hiltbrunner, A., Wigge, P.A.,**

705 **Schäfer, E., Vierstra, R.D., and Casal, J.J.** (2016). Phytochrome B integrates light and
706 temperature signals in Arabidopsis. Science (80-.).

707 **Liu, Q. et al.** (2017). Molecular basis for blue light-dependent phosphorylation of Arabidopsis
708 cryptochrome 2. Nat. Commun.

709 **Marondedze, C., Groen, A.J., Thomas, L., Lilley, K.S., and Gehring, C.** (2016). A
710 Quantitative Phosphoproteome Analysis of cGMP-Dependent Cellular Responses in
711 Arabidopsis thaliana. Mol. Plant.

712 **Medzihradszky, M. et al.** (2013). Phosphorylation of Phytochrome B Inhibits Light-Induced
713 Signaling via Accelerated Dark Reversion in Arabidopsis. Plant Cell.

714 **Ni, W., Xu, S.-L., González-Grandío, E., Chalkley, R.J., Huhmer, A.F.R., Burlingame, A.L.,**
715 **Wang, Z.-Y., and Quail, P.H.** (2017). PPKs mediate direct signal transfer from
716 phytochrome photoreceptors to transcription factor PIF3. Nat. Commun.

717 **Nito, K., Wong, C.C.L., Yates, J.R., and Chory, J.** (2013). Tyrosine Phosphorylation
718 Regulates the Activity of Phytochrome Photoreceptors. Cell Rep.

719 **Ohtsubo, T., Matsuda, O., Iba, K., Terashima, I., Sekiguchi, M., and Nakabeppu, Y.** (1998).
720 Molecular cloning of AtMMH, an Arabidopsis thaliana ortholog of the Escherichia coli mutM
721 gene, and analysis of functional domains of its product. Mol. Gen. Genet.

722 **Portolés, S. and Más, P.** (2010). The functional interplay between protein kinase CK2 and cca1
723 transcriptional activity is essential for clock temperature compensation in Arabidopsis.
724 PLoS Genet.

725 **Probst, A. V. and Mittelsten Scheid, O.** (2015). Stress-induced structural changes in plant
726 chromatin. Curr. Opin. Plant Biol.

727 **Rademacher, E.H. and Offringa, R.** (2012). Evolutionary Adaptations of Plant AGC Kinases:

728 From Light Signaling to Cell Polarity Regulation. Front. Plant Sci.

729 **Reimand, J., Arak, T., Adler, P., Kolberg, L., Reisberg, S., Peterson, H., and Vilo, J.** (2016).
730 g:Profiler-a web server for functional interpretation of gene lists (2016 update). Nucleic
731 Acids Res.

732 **Rosa, S. and Shaw, P.** (2013). Insights into Chromatin Structure and Dynamics in Plants.
733 Biology (Basel).

734 **Roy, S., Choudhury, S.R., Sengupta, D.N., and Das, K.P.** (2013). Involvement of AtPol in the
735 Repair of High Salt- and DNA Cross-Linking Agent-Induced Double Strand Breaks in
736 Arabidopsis. PLANT Physiol.

737 **Sakamoto, Y. and Takagi, S.** (2013). LITTLE NUCLEI 1 and 4 regulate nuclear morphology in
738 arabidopsis thaliana. Plant Cell Physiol.

739 **Schwartz, D. and Gygi, S.P.** (2005). An iterative statistical approach to the identification of
740 protein phosphorylation motifs from large-scale data sets. Nat. Biotechnol.

741 **Silva-Sanchez, C., Li, H., and Chen, S.** (2015). Recent advances and challenges in plant
742 phosphoproteomics. Proteomics.

743 **Sønderby, I.E., Geu-Flores, F., and Halkier, B.A.** (2010). Biosynthesis of glucosinolates--gene
744 discovery and beyond. Trends Plant Sci.

745 **Su, Y., Wang, S., Zhang, F., Zheng, H., Liu, Y., Huang, T., and Ding, Y.** (2017).
746 Phosphorylation of Histone H2A at Serine 95: A Plant-specific Mark Involved in Flowering
747 Time Regulation and H2A.Z Deposition. Plant Cell.

748 **Sugiyama, N., Nakagami, H., Mochida, K., Daudi, A., Tomita, M., Shirasu, K., and**
749 **Ishihama, Y.** (2008). Large-scale phosphorylation mapping reveals the extent of tyrosine
750 phosphorylation in Arabidopsis. Mol. Syst. Biol.

751 **Supek, F., Bošnjak, M., Škunca, N., and Šmuc, T.** (2011). Revigo summarizes and visualizes
752 long lists of gene ontology terms. PLoS One.

753 **Suzuki, K., Sako, K., Akiyama, K., Isoda, M., Senoo, C., Nakajo, N., and Sagata, N.** (2015).
754 Identification of non-Ser/Thr-Pro consensus motifs for Cdk1 and their roles in mitotic
755 regulation of C2H2 zinc finger proteins and Ect2. Sci. Rep.

756 **Tessadori, F. et al.** (2009). PHYTOCHROME B and HISTONE DEACETYLASE 6 control light-
757 induced chromatin compaction in Arabidopsis thaliana. PLoS Genet.

758 **Vergara, Z. and Gutierrez, C.** (2017). Emerging roles of chromatin in the maintenance of
759 genome organization and function in plants. Genome Biol.

760 **Vlastaridis, P., Kyriakidou, P., Chaliotis, A., Van de Peer, Y., Oliver, S.G., and Amoutzias,**
761 **G.D.** (2017). Estimating the total number of phosphoproteins and phosphorylation sites in
762 eukaryotic proteomes. Gigascience.

763 **Wang, H., Dittmer, T.A., and Richards, E.J.** (2013). Arabidopsis CROWDED NUCLEI (CRWN)
764 proteins are required for nuclear size control and heterochromatin organization. BMC Plant
765 Biol.

766 **Wang, Y., Liu, Z., Cheng, H., Gao, T., Pan, Z., Yang, Q., Guo, A., and Xue, Y.** (2014). EKPD:
767 A hierarchical database of eukaryotic protein kinases and protein phosphatases. Nucleic
768 Acids Res.

769 **Wang, Z., Casas-Mollano, J.A., Xu, J., Riethoven, J.-J.M., Zhang, C., and Cerutti, H.**
770 (2015a). Osmotic stress induces phosphorylation of histone H3 at threonine 3 in
771 pericentromeric regions of Arabidopsis thaliana. Proc. Natl. Acad. Sci. U. S. A.

772 **Wang, Z., Yang, R., Guo, L., Fang, M., Zhou, Y., and Gu, Z.** (2015b). Effects of abscisic acid
773 on glucosinolate content, isothiocyanate formation and myrosinase activity in cabbage

774 sprouts. Int. J. Food Sci. Technol.

775 **West, C.E., Waterworth, W.M., Jiang, Q., and Bray, C.M.** (2000). Arabidopsis DNA ligase IV
776 is induced by γ-irradiation and interacts with an Arabidopsis homologue of the double
777 strand break repair protein XRCC4. Plant J.

778 **van Wijk, K.J., Friso, G., Walther, D., and Schulze, W.X.** (2014). Meta-Analysis of
779 Arabidopsis thaliana Phospho-Proteomics Data Reveals Compartmentalization of
780 Phosphorylation Motifs. Plant Cell.

781 **Yuan, D., Lai, J., Xu, P., Zhang, S., Zhang, J., Li, C., Wang, Y., Du, J., Liu, Y., and Yang, C.**
782 (2014). AtMMS21 regulates DNA damage response and homologous recombination repair
783 in Arabidopsis. DNA Repair (Amst).

784 **van Zanten, M., Tessadori, F., McLoughlin, F., Smith, R., Millenaar, F.F., van Driel, R.,**
785 **Voesenek, L.A.C.J., Peeters, A.J.M., and Fransz, P.** (2010). Photoreceptors
786 CRYTOCHROME2 and Phytochrome B Control Chromatin Compaction in Arabidopsis.
787 PLANT Physiol.

788 **Zheng, H., Zhang, F., Wang, S., Su, Y., Jiang, P., Cheng, R., Ji, X., Hou, S., and Ding, Y.**
789 (2017). MLK1 and MLK2 coordinate RGA and CCA1 activity to regulate hypocotyl
790 elongation in Arabidopsis thaliana. Plant Cell.

791 **Zhu, M. and Assmann, S.M.** (2017). Metabolic Signatures in Response to Abscisic Acid (ABA)
792 Treatment in Brassica napus Guard Cells Revealed by Metabolomics. Sci. Rep.

793

794

795

796 **Figure Legends**

797 **Figure 1. Schematic Representation of the Quantitative Proteomics Workflow**

798 Tissue samples were collected at ZT12 and ZT14 from wild type and mutant seedlings entrained
799 with a 12L:12D light/dark cycle (1). Total protein was extracted and digested (2). Following
800 TMT10plex isobaric labeling (3), samples were subjected to high pH reversed phase
801 prefractionation (5). Phosphopeptides were enriched using a TiO2-based method (4). Both
802 phosphopeptide-enriched and global samples were analyzed by LC-MS/MS (6).

803 **Figure 2. Global Proteomic Analysis of *mlk* Mutant Seedlings**

804 Volcano plots of peptides identified in mutant and wild-type seedlings at ZT12 and ZT14. The
805 x-axis specifies the log2 fold-change (FC) of mutant/wild-type and the y-axis specifies the
806 negative logarithm to the base 10 of the t-test p-values. Open circles represent individual
807 peptides, with blue circles specifying those considered statistically significant. Black vertical
808 and horizontal lines reflect the filtering criteria (log2 FC = ±1 and p-value = 0.05) for
809 significance.

810 **Figure 3. Analysis of Quantitative Phosphoproteomics of *mlk* Mutant Seedlings**

811 (A) The distribution of threonine (T), serine (S), and tyrosine (Y) phosphorylation sites identified
812 at ZT12 and ZT14. (B) Volcano plot of phosphopeptides identified in mutant and wild-type
813 seedlings at ZT12 and ZT14. The x-axis specifies the log2 fold-change (FC) of mutant/wild-
814 type and the y-axis specifies the negative logarithm to the base 10 of the t-test p-values. Open
815 circles represent individual peptides, with blue circles specifying those considered statistically
816 significant. Black vertical and horizontal lines reflect the filtering criteria (log2 FC = ±0.585 and
817 p-value = 0.05) for significance. (C and D) Size-proportional Venn diagrams of differentially
818 regulated phosphoproteins in *mlk1/2/3* and *mlk1/3/4* mutants at ZT12 (C) and ZT14 (D).
819 Numbers indicate unique phosphoproteins.

820 **Figure 4. Motif Analysis of Differentially Phosphorylated Peptides**

821 Phosphopeptides with altered abundance in *mlk1/3/4* mutants at ZT12 (A) and ZT14 (B) where
822 extended (http://schwartzlab.uconn.edu/pepextend) and centered. Motif-X analysis was then
823 preformed with the probability threshold was set to p-value ≤ 10^{-6}, the occurrence threshold
824 was set to 20, and the default IPI Arabidopsis Proteome data set was used as the background
825 data set.

826 **Figure 5. Gene Ontology (GO) Enrichment Analysis**

827 GO enrichment analysis of proteins identified as having increased (A) or decreased (B)
828 abundance in *mlk* mutant seedlings at indicated ZTs when compared to wild-type. Cluster
829 representative GO terms identified with REVIGO (semantic similarity threshold < 0.7) in the
830 category of Biological Process are shown.

831 **Figure 6. *mlk* Mutant Seedlings Contain Elevated Levels of MET Derived Glucosinolates**

832 Glucosinolate (GLS) content of 10 day old mutant and wild type seedlings at ZT12 was
833 quantified using HPLC. GLS identity determined using UV spectra and confirmed by LC-
834 MS/MS. The average of 4 biological replicates is presented. Error bars indicate standard
835 deviation. *P<0.01, compared with wild type seedlings (Student's *t*-test).

836 **Figure 7. Gene Ontology Enrichment Analysis of Differentially Phosphorylated Proteins**

837 (A) Heat map showing the p-value significance of enriched cellular component GO categories
838 of proteins with altered abundance in *mlk* mutant seedlings at ZT12 and ZT14. (B and C)
839 Treemap representation of Biological Process GO categories enriched in *mlk1/3/4* mutant
840 seedlings at ZT12 (B) and ZT14 (C). The box size correlates to the –log10 *P*-value of the GO-
841 term enrichment. Boxes with the same color indicate related GO-terms and correspond to the

842 representative GO-term which is found in the upper-left of each box. REVIGO was used to
843 eliminate redundant GO-terms with a dispensability value ≥ 0.7 (A) or ≥ 0.5 (B and C).

844 **Figure 8. Analysis of Differentially Phosphorylated Peptides in *mlk1/3/4* Mutants at ZT12**

845 (A) Size-proportional Venn diagram of proteins which show increased, decreased, or both
846 increased and decreased abundance of identified phosphosites in *mlk1/3/4* mutant seedlings
847 at ZT12. Numbers indicate unique phosphoproteins. Analysis of phosphoproteins that show
848 increased (B) or decreased (C) in abundance in the *mlk1/3/4* mutant seedlings background at
849 ZT12. Treemap representations of Biological Process GO category enrichment are shown. The
850 box size correlates to the –log10 *P*-value of the GO-term enrichment. Boxes with the same color
851 indicate related GO-terms and correspond to the representative GO-term which is found in the
852 upper-left of each box. REVIGO was used to eliminate redundant GO-terms with a dispensability
853 value ≥ 0.5.

854 **Figure 9. *mlk1/3/4* Mutants Have Increased Sensitivity to MMS Treatment**

855 (A) Representative images of mutant and wild type seedlings 15 days after transfer to solid
856 media containing the indicated concentration of MMS. Chlorotic tissue is indicated with a blue
857 arrowhead. Scale bar = 5 mm. (B) Fresh weight of 21-day old wild type and mutant seedlings
858 grown in the presence of MMS relative to mock treated samples. The average of 3 biological
859 replicates of ≥10 seedlings each is presented. (C) Percent of seedlings exhibiting post-
860 germination developmental arrest after 12 days of growth in the presence of 150 PMM MMS.
861 The average of 3 biological replicates of ≥30 seedlings is presented. (B and C) Error bars
862 indicate standard deviation. *$P<0.05$, **$P<0.01$compared with wild type seedlings (Student's *t*-
863 test). (D) Representative images of mutant and wild type seedlings germinated in the presence
864 of 150 PPM MMS. (E) Representative images of mutant and wild type seedlings irradiated with
865 indicated levels of UV-C. Scale bar = 2 mm.

866

867

868

869

870

871

872

Table 1. Phosphosites Identified in Circadian-Associated Proteins.

Protein Group Accession	Protein Names	Protein Description	Peptide Sequence	Log2 FC	P-Value
AT2G18790	PHYB	phytochrome B	GGEQAQSSGT^{42}K	-1.36	5.95E-06
AT4G30200	VEL1	vernalization5/VIN3-like protein	KPS^{506}SKNEDNNSPSVDESAAK	-0.89	3.00E-02
AT5G11260	HY5	Basic-leucine zipper (bZIP) transcription factor family protein	ESGSAT^{64}GQER	-0.81	1.46E-02
AT3G22380	TIC	time for coffee	MPS^{324}TSKQEAAGNDLTEAAK	-0.79	1.98E-04
AT5G02810	PRR7	pseudo-response regulator 7	QDNS^{355}FEK	-0.74	1.04E-05
AT2G17840	ERD7	Senescence/dehydration-associated protein-like protein	SAAS^{488}QKK	-0.69	3.95E-02
AT5G02810	PRR7	pseudo-response regulator 7	AVS^{275}LWDR	-0.62	1.93E-03
AT4G30200	VEL1	vernalization5/VIN3-like protein	LCSSALESLETIAT^{330}TPPDVAALPS^{340}PR	0.61	1.53E-02
AT4G30200	VEL1	vernalization5/VIN3-like protein	NEDNNSPS^{516}VDESAAK	0.63	1.01E-04
AT5G52310	LTI78	low-temperature-responsive protein 78 (LTI78) / desiccation-responsive protein 29A (RD29A)	NEYSPES^{387}DGGLGAPLGGNFPVR	0.64	6.53E-03
AT3G09600	RVE8	Homeodomain-like superfamily protein	GLLNVSSPSTSGMGSSSR	0.83	1.72E-03
AT3G46780	PTAC16	plastid transcriptionally active 16	ADAVGVT^{410}VDGLFNK	0.95	9.29E-03

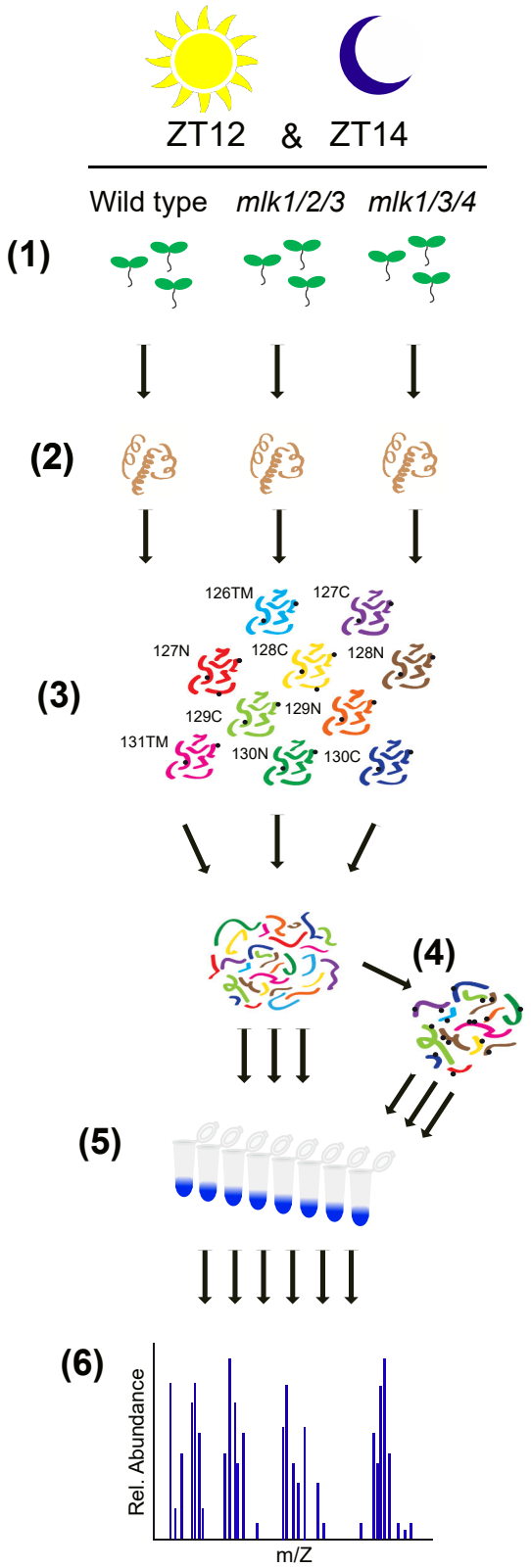

Figure 1. Schematic Representation of the Quantitative Proteomics Workflow

Tissue samples were collected at ZT12 and ZT14 from wild type and mutant seedlings entrained with at 12L:12D light cycle (1). Total protein was extracted and digested (2). Following TMT10plex isobaric labeling (3), samples were subjected to high pH reversed phase prefractionation (5). Phosphopeptides were enriched using a TiO2-based method (4). Both phosphopeptide-enriched and global samples were analyzed by LC-MS/MS (6).

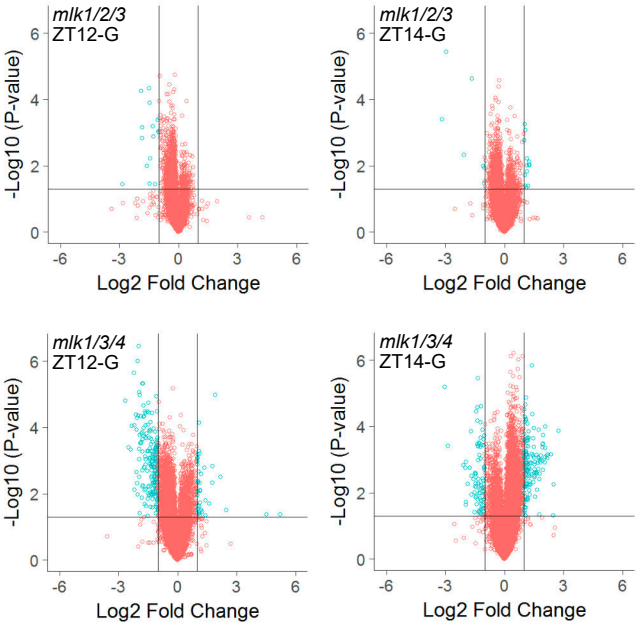

Figure 2. Global Proteomic Analysis of *mlk* Mutant Seedlings

Volcano plots of peptides identified in mutant and wild-type seedlings at ZT12 and ZT14. The x-axis specifies the log2 fold-change (FC) of mutant/wild-type and the y-axis specifies the negative logarithm to the base 10 of the t-test p-values. Open circles represent individual peptides, with blue circles specifying those considered statistically significant. Black vertical and horizontal lines reflect the filtering criteria (log2 FC = ±1 and p-value = 0.05) for significance.

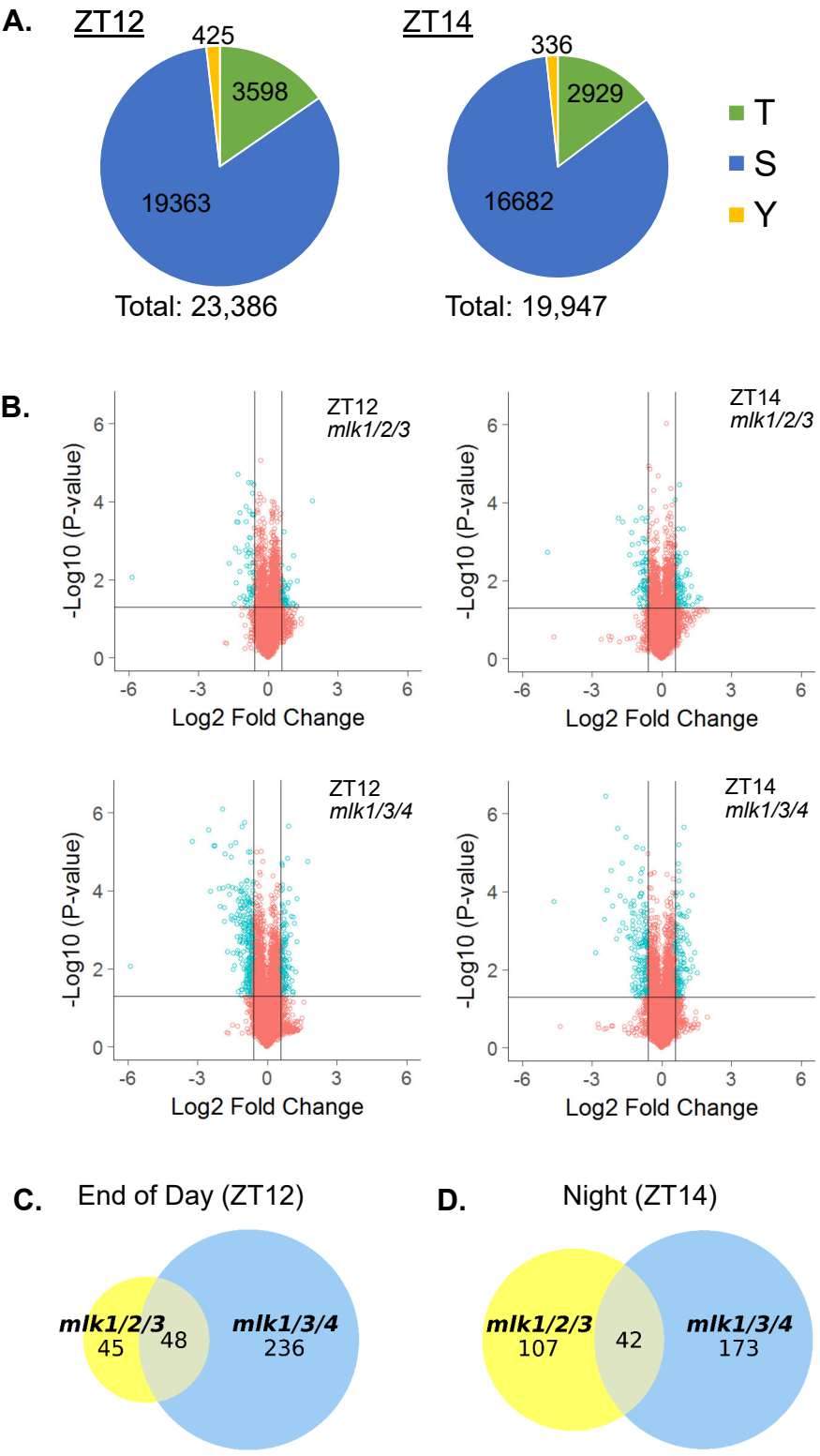

Figure 3. Analysis of Quantitative Phosphoproteomics of *mlk* Mutant Seedlings

(A) The distribution of threonine (T), serine (S), and tyrosine (Y) phosphorylation sites identified at ZT12 and ZT14. (B) Volcano plot of phosphopeptides identified in mutant and wild-type seedlings at ZT12 and ZT14. The x-axis specifies the log2 fold-change (FC) of mutant/wild-type and the y-axis specifies the negative logarithm to the base 10 of the t-test p-values. Open circles represent individual peptides, with blue circles specifying those considered statistically significant. Black vertical and horizontal lines reflect the filtering criteria (log2 FC = ±0.585 and p-value = 0.05) for significance. (C and D) Size-proportional Venn diagrams of differentially regulated phosphoproteins in *mlk1/2/3* and *mlk1/3/4* mutants at ZT12 (C) and ZT14 (D). Numbers indicate unique phosphoproteins.

A.

	#	Motif	Motif Score	Foreground Matches	Foreground Size	Background Matches	Background Size	Fold Increase
Decreased	1	.....S..K....	10.36	38	188	60894	1013104	3.36
	2	....R..S.....	5.09	23	150	52253	952210	2.79
	3	....K..S.....	5.02	22	127	55173	899957	2.83
Increased	1	.....SP.....	10.53	42	250	53111	1013104	3.2
	2	.....S.S.....	6.52	51	208	113600	959993	2.07

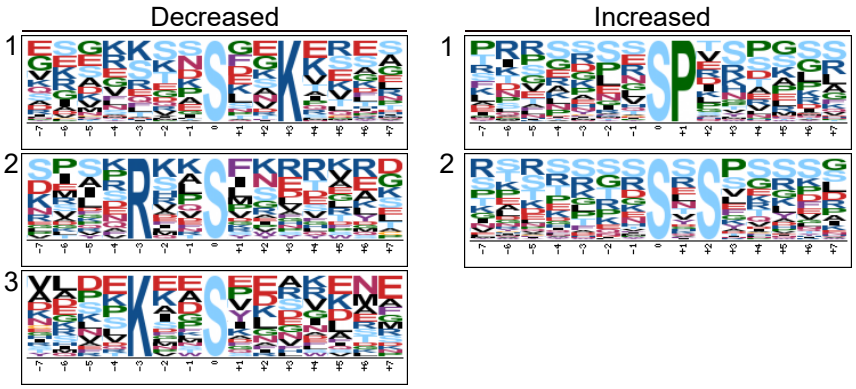

B.

	#	Motif	Motif Score	Foreground Matches	Foreground Size	Background Matches	Background Size	Fold Increase
Decreased	1	.....S.....E.	6.15	27	149	63949	1013104	2.87
	2	....K..S.....	5.12	21	122	55198	949155	2.96
Increased	1	.....SP.....	11.64	25	88	53111	1013104	5.42

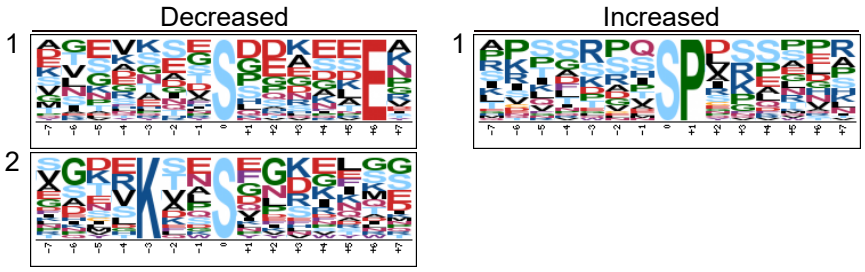

Figure 4. Motif Analysis of Differentially Phosphorylated Peptides

Phosphopeptides with altered abundance in *mlk1/3/4* mutants at ZT12 (A) and ZT14 (B) where extended (http://schwartzlab.uconn.edu/pepextend) and centered. Motif-X analysis was then preformed with the probability threshold was set to p-value ≤ 10^{-6}, the occurrence threshold was set to 20, and the default IPI Arabidopsis Proteome data set was used as the background data set.

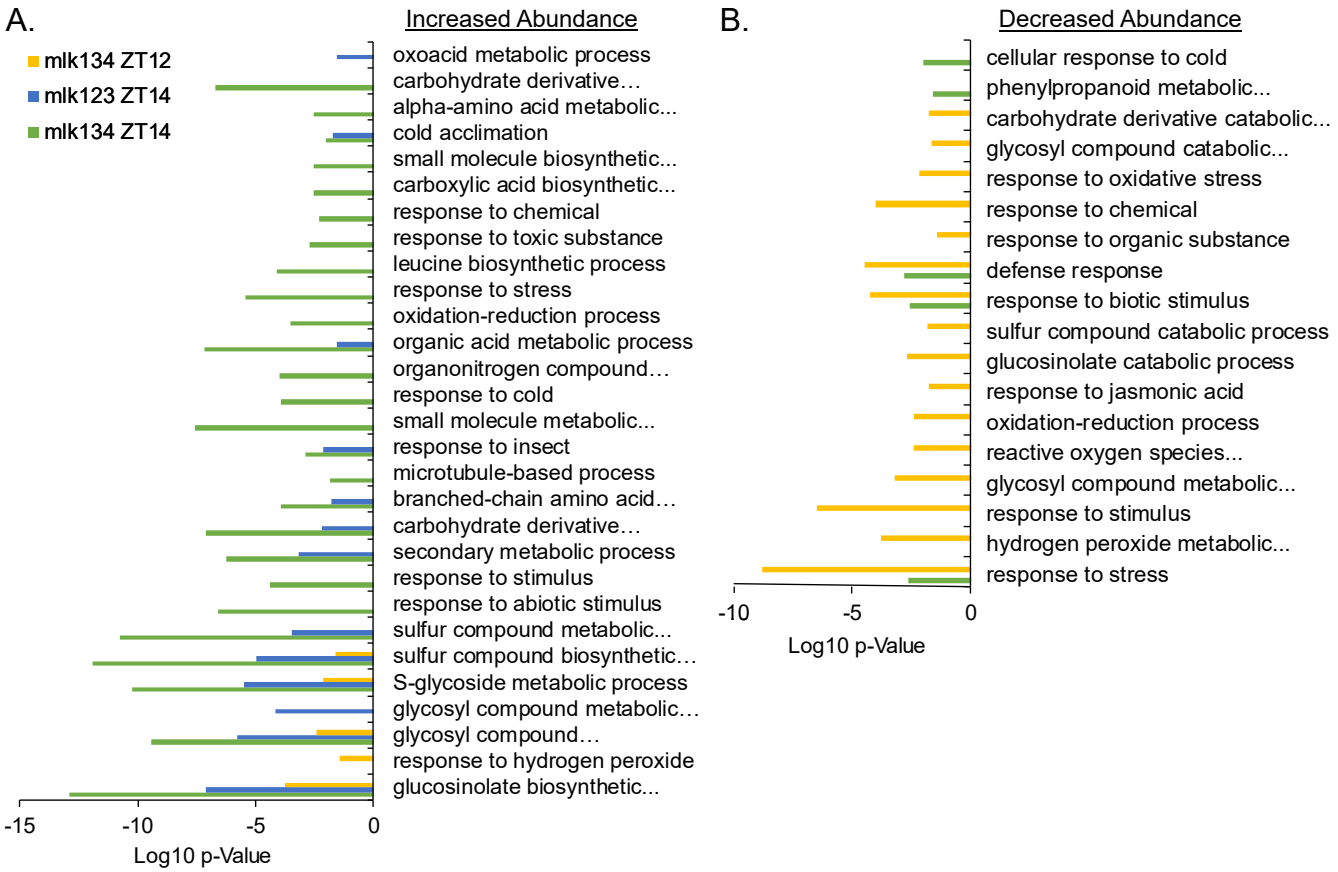

Figure 5. Gene Ontology (GO) Enrichment Analysis

GO enrichment analysis of proteins identified as having increased (A) or decreased (B) abundance in *mlk* mutant seedlings at indicated ZTs when compared to wild-type. Cluster representative GO terms identified with REVIGO (semantic similarity threshold < 0.7) in the category of Biological Process are shown.

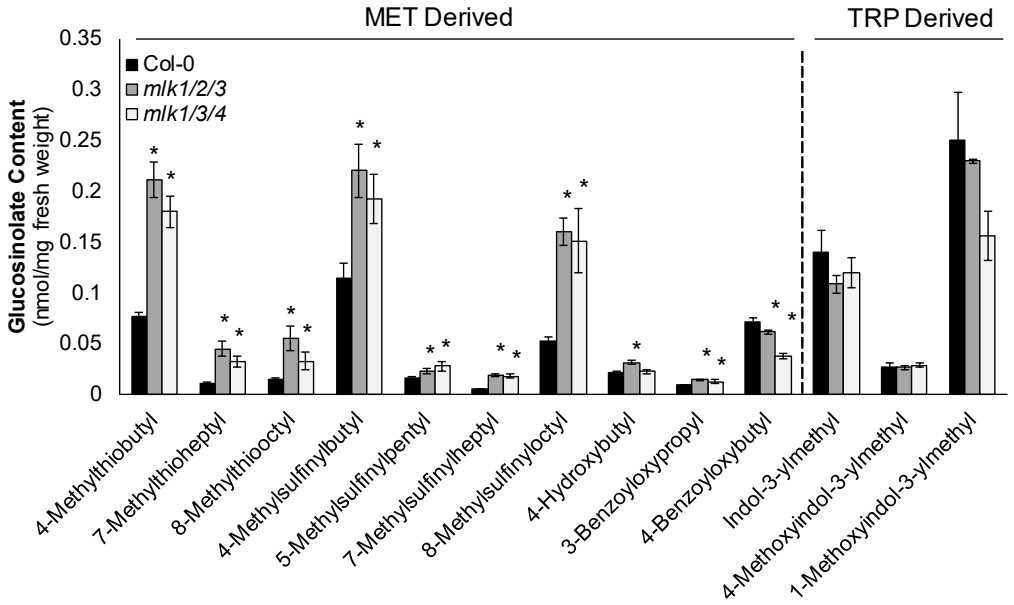

Figure 6. *mlk* Mutant Seedlings Contain Elevated Levels of MET Derived Glucosinolates

Glucosinolate (GLS) content of 10 day old mutant and wild type seedlings at ZT12 was quantified using HPLC. GLS identity determined using UV spectra and confirmed by LC-MS/MS. The average of 4 biological replicates is presented. Error bars indicate standard deviation. *P<0.01, compared with wild type seedlings (Student's *t*-test).

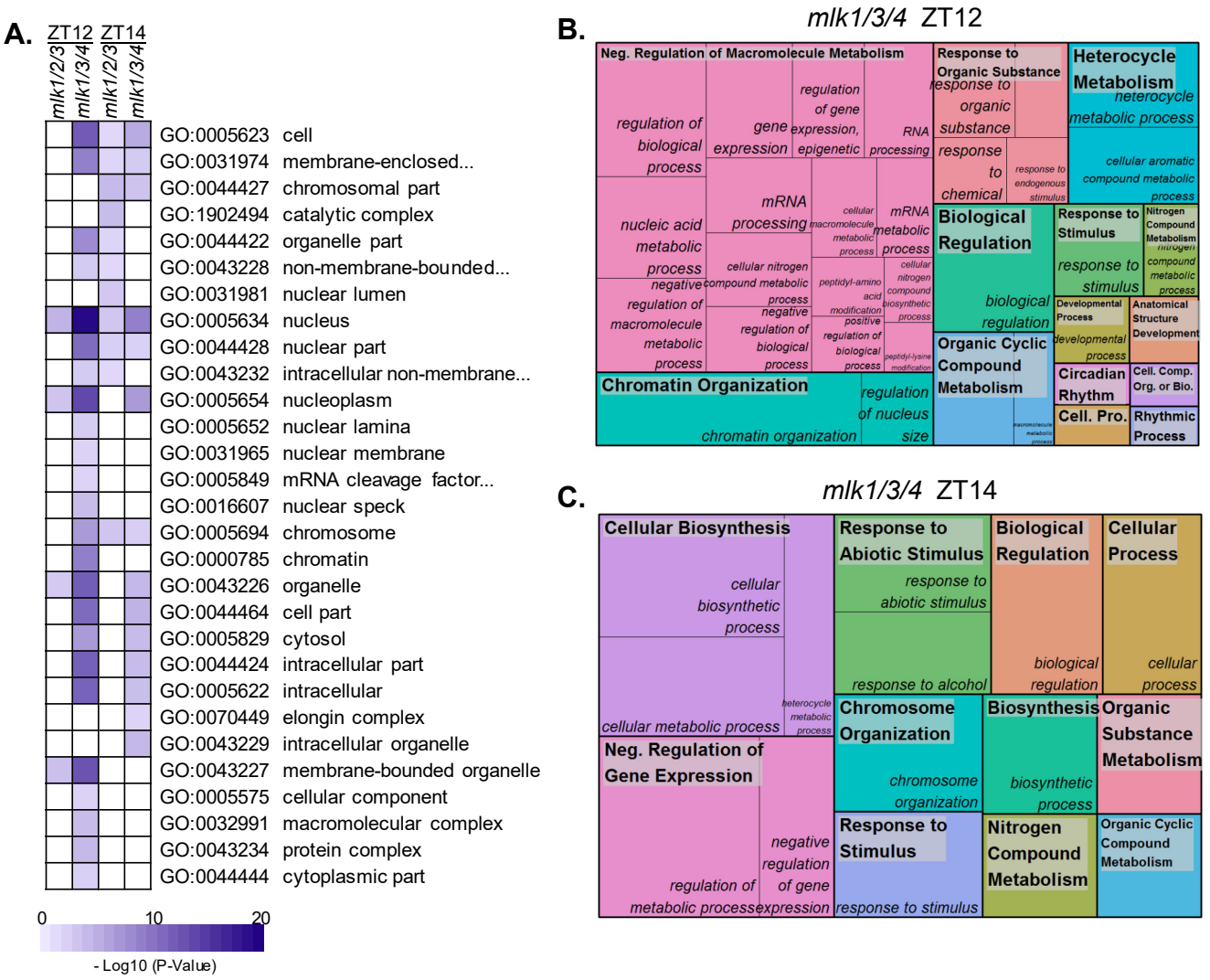

Figure 7. Gene Ontology Enrichment Analysis of Differentially Phosphorylated Proteins

(A) Heat map showing the p-value significance of enriched cellular component GO categories of proteins with altered abundance in *mlk* mutant seedlings at ZT12 and ZT14. (B and C) Treemap representation of Biological Process GO categories enriched in *mlk1/3/4* mutant seedlings at ZT12 (B) and ZT14 (C). The box size correlates to the –log10 *P*-value of the GO-term enrichment. Boxes with the same color indicate related GO-terms and correspond to the representative GO-term which is found in the upper-left of each box. REVIGO was used to eliminate redundant GO-terms with a dispensability value ≥ 0.7 (A) or ≥ 0.5 (B and C).

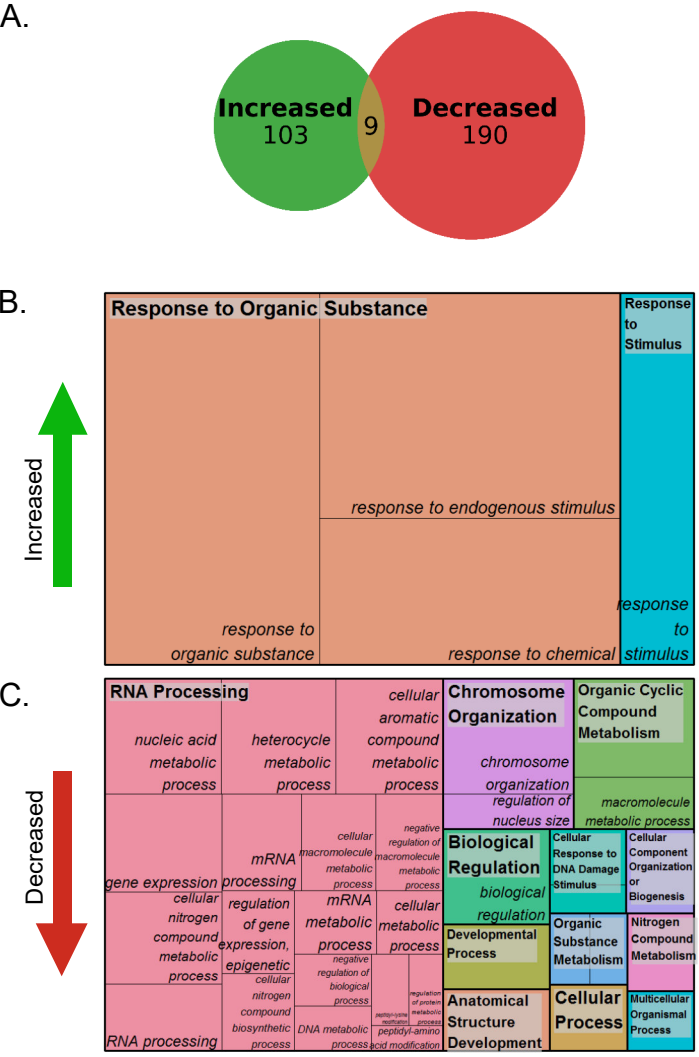

Figure 8. Analysis of Differentially Phosphorylated Peptides in *mlk1/3/4* Mutants at ZT12

(A) Size-proportional Venn diagram of proteins which show increased, decreased, or both increased and decreased abundance of identified phosphosites in *mlk1/3/4* mutant seedlings at ZT12. Numbers indicate unique phosphoproteins. Analysis of phosphoproteins that show increased (B) or decreased (C) in abundance in the *mlk1/3/4* mutant seedlings background at ZT12. Treemap representations of Biological Process GO category enrichment are shown. The box size correlates to the –log10 *P*-value of the GO-term enrichment. Boxes with the same color indicate related GO-terms and correspond to the representative GO-term which is found in the upper-left of each box. REVIGO was used to eliminate redundant GO-terms with a dispensability value ≥ 0.5.

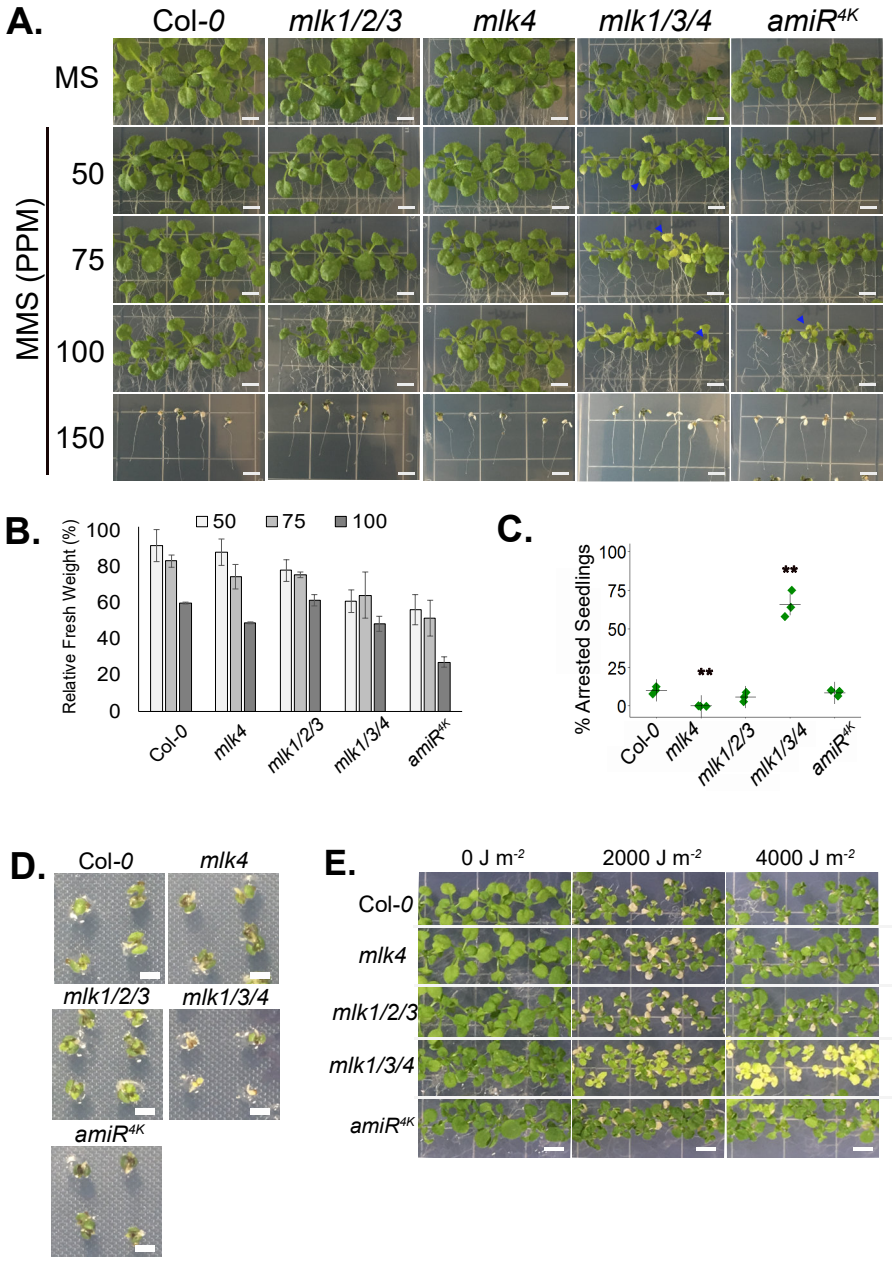

Figure 9. *mlk1/3/4* Mutants Have Increased Sensitivity to MMS Treatment

(A) Representative images of mutant and wild type seedlings 15 days after transfer to solid media containing the indicated concentration of MMS. Chlorotic tissue is indicated with a blue arrowhead. Scale bar = 5 mm. (B) Fresh weight of 21-day old wild type and mutant seedlings grown in the presence of MMS relative to mock treated samples. The average of 3 biological replicates of ≥10 seedlings each is presented. (C) Percent of seedlings exhibiting post-germination developmental arrest after 12 days of growth in the presence of 150 PMM MMS. The average of 3 biological replicates of ≥30 seedlings is presented. (B and C) Error bars indicate standard deviation. *P<0.05, **P<0.01compared with wild type seedlings (Student's t-test). (D) Representative images of mutant and wild type seedlings germinated in the presence of 150 PPM MMS. (E) Representative images of mutant and wild type seedlings irradiated with indicated levels of UV-C. Scale bar = 2 mm.